Vol. 8: 61-87, 1997 | CLIMATE RESEARCH Clim Res | Published March 27

The Frankfurt Biosphere Model: a global process-oriented model of seasonal and long-term CO_2 exchange between terrestrial ecosystems and the atmosphere. II. Global results for potential vegetation in an assumed equilibrium state

Gundolf H. Kohlmaier[1,*], Franz-W. Badeck[2], Ralf D. Otto[1], Christof Häger[1], Silke Dönges[1], Jürgen Kindermann[1], Gudrun Würth[1], Torsten Lang[1], Ulrich Jäkel[1], Andreas Nadler[1], Peter Ramge[1], Axel Klaudius[1], Stefan Habermehl[1], Matthias K. B. Lüdeke[3]

[1]Institut für Physikalische und Theoretische Chemie, J. W. Goethe-Universität Frankfurt am Main, Marie-Curie-Str. 11, D-60439 Frankfurt am Main, Germany

[2]Laboratoire d'Ecophysiologie Végétale, Université de Paris Sud XI, Orsay, France

[3]Potsdam Institut für Klimafolgenforschung, Telegrafenberg, Postfach 601203, D-14412 Potsdam, Germany

ABSTRACT: Regional variability and seasonal courses of atmospheric CO_2 provide important clues to the understanding of the carbon exchange fluxes which determine the global carbon budget. We apply the Frankfurt Biosphere Model (FBM) to all 32 vegetation types of a modified global Matthews' vegetation map, simulating seasonal carbon exchange fluxes of the terrestrial ecosystems and their geographical variability on a global scale. For each 0.5° by 0.5° grid element the model calculates gross photosynthesis of the canopy and autotrophic respiration on an hourly time step, and heterotrophic respiration as well as the model-compartment sizes and LAI (leaf area index) on a daily time step. The driving variables temperature, irradiation, and soil moisture are derived from the Cramer and Leemans database. Soil moisture is calculated by an improved bucket model in which the soil properties given by the FAO soil map are combined with the rooting depth of different vegetation types to deduce the available water capacity and the permanent wilting point. Based on mean estimates of ecological variables [e.g. net primary production (NPP), biomass and soil carbon] and a characteristic seasonal climate, the free parameters of each vegetation type are calibrated. With these parameters, taking the climate variation within the vegetation types into account, the seasonal courses of NPP are calculated, summing up to a global annual integral of 50.3 Gt C yr^{-1}. The results are presented in the form of a world map showing the annual NPP and a table with monthly values of NPP averaged over 5° latitude belts. The latter results are graphically displayed not only for NPP but also for heterotrophic respiration and the resulting seasonal net ecosystem production. Since the FBM keeps track of the seasonal development of leaf biomass, the corresponding seasonal LAI is examined for each grid element. The calculated leaf emergence dates are in good agreement with observations from phenological gardens as well as with NDVI (normalized difference vegitation index) derived phenology.

KEY WORDS: Carbon balance · Terrestrial ecosystems · Global simulation model · Allocation and phenology · Primary production · Leaf area index · CO_2 exchange fluxes

1. INTRODUCTION

Climate in interaction with the biosphere determines the performance of ecosystems as an important part of biogeochemical cycles. Changes in the partial pressure of atmospheric greenhouse gases and their possible consequences for the climate system have especially led to an intensification of research on the global carbon cycle. During the last 5 yr several models have been developed in order to quantify the metabolism of

*E-mail: g.kohlmaier@chemie.uni-frankfurt.de

terrestrial ecosystems and their CO_2 exchange with the atmosphere at a global scale. Among the large number of globally applicable biosphere models there is great diversity with respect to model structure, the quantitative functions used, and the results. Therefore a detailed intercomparison of biosphere models was performed at a workshop in Potsdam, Germany, in 1995 (A. Fischer & J Kaduk unpubl.), as part of which the simulated monthly net primary production of 17 models was analysed. Due to the variety of model characteristics the models were classified into a number of categories to make the comparisons more reliable and clear.

The first category contains correlative models based on the MIAMI model (Lieth 1975), the oldest representative of NPP (net primary productivity) models. Correlative models such as the High Resolution Biosphere Model (HRBM; Esser et al. 1994), which is the most recent version of the MIAMI model, statistically relate annual values of temperature and precipitation to values of NPP and derive the seasonal distribution of NPP via the potential evapotranspiration.

In the second category of terrestrial biosphere models, monthly NDVI (normalized difference vegetation index) composites are used as an input. These models are described as being diagnostic because they require actually measured information about the state of the biosphere, i.e. the absorbed photosynthetically active radiation (APAR), and apply a light-use efficiency variable ε to determine the production from APAR (e.g. CASA; Potter et al. 1993).

The final category comprises 2 different classes of mechanistic models which simulate the physiological processes involved in the flux exchanges between atmosphere, biosphere and soil. The first class contains models which attempt to couple the vegetation structure and the CO_2, water and energy fluxes, such as the BIOME2 model (Haxeltine et al. in press). Models in the second class, on the other hand, mechanistically estimate seasonal biogeochemical fluxes for a prescribed vegetation type. Within this last category, the Terrestrial Ecosystem Model (TEM) developed by Melillo et al. (1993) simulates the monthly fluxes between the different carbon and nitrogen pools and their dependence on the climate variables. Other models such as the BIOME-BGC (Running & Hunt 1993) also simulate the fluxes for a given vegetation but additionally force the seasonal behaviour of the canopy through interpretation of satellite observations. A third group of models with a prescribed vegetation map calculate the seasonal behaviour of both the exchange fluxes and the canopy. The FBM (Frankfurt Biosphere Model), together with the CARAIB (Warnant et al. 1994), SILVAN (Kaduk & Heimann 1996) and PLAI (Plöchl & Cramer 1995) models, belongs to this last group of models. To work properly, biogeochemical models like the FBM must be initialized with the natural distribution of vegetation types, either as calculated from a vegetation model or derived from reconstruction of the present to preindustrial times.

The FBM was developed as a process-oriented ecophysiological model capable of calculating carbon exchange fluxes with a temporal resolution of days/hours. The essential structure of the FBM was built as simply as possible and as elaborately as necessary in order to construct a model that follows 2 basic ecological hypotheses: the vegetation tends to maximize the photosynthesizing tissue, and for a given mass of photosynthetically active material there exists a minimum requirement of supporting (structural) biomass. This basic structure enables the model to represent important features of an ecosystem, such as growth, phenology and allocation strategy, with all these features governed by physiological processes driven by climatic variables. The strictly state-dependent growth of the vegetation allows the model to simulate the transient response to climate variability as well as growth from any initial state.

This basic structure of a biosphere model, in which an allocator dividing the photosynthesized material into 2 different compartments is included, was first published in 1989 by Janecek et al. Since then a number of physiology-based biosphere models have incorporated some derivative of this allocator. Recently Kaduk & Heimann (1996) published a model in which a similar allocation strategy for assimilated material is used.

As described by Kindermann et al. (1993) and Lüdeke et al. (1994, 1995) the basic structure of the FBM is valid for all plant functional types and is applicable at a global scale. In an earlier study we reported steady state results for 2 major forest vegetation types of the boreal and temperate zone (Lüdeke et al. 1994); we now present global results of steady-state simulations with the FBM. Among the various possible output values, the temporal dynamics and spatial distribution of NPP and leaf area index (LAI) are the most significant results to be discussed.

The FBM offers the unique possibility of predicting the seasonal behaviour of CO_2 exchange between ecosystems and the atmosphere solely as a function of the climate parameters characteristic for the different locations of the globe. It can be checked against the data from phenology gardens (Schnelle 1985) and against observations from space by evaluation of the NDVI (Lüdeke et al. 1996). Finally, it can be coupled with an atmospheric transport model where the seasonal and regional source-sink function can be verified by the regionally different seasonal atmospheric CO_2 concentrations. As the FBM directly couples seasonal behaviour with the long-term behaviour of perennial plant communities, it can equally predict the observed

interannual CO_2 variations as a function of the changed weather patterns occurring from year to year (Kindermann et al. 1996). Its correct prediction of the seasonal and interannual behaviour leads us to hope that very long-term behaviour can also be predicted fairly well. As stated above, the FBM can be run in a transient and in a steady state mode with respect to the biosphere compartments. In this publication we focus our attention on the steady state results for potential vegetation undisturbed by human interaction.

2. MODEL DESCRIPTION

The development of the FBM started out with the subdivision of living vegetation into 2 compartments (see Fig. 1) and the allometric scheme presented by Janecek et al. (1989). After adding a module for the calculation of heterotrophic respiration based on Fung et al. (1987) and setting up an initial version of modules to represent global data layers of vegetation (Matthews 1983) and climate (Shea 1986), we presented the first global version of the FBM (FBM 1.0) at the 1991 NATO summer school in Il Ciocco (Italy). FBM version 2.0 is described in Kindermann et al. (1993) and Lüdeke et al. (1994). This version includes the distinction between cold and drought deciduous leaf turnover types, a separate simple bucket model for the calculation of the soil moisture content, and modifications of the temperature response of photosynthetic productivity. Furthermore Matthews' vegetation map is extended by explicitly considering C_3 and C_4 grasslands.

We start by summarizing the most important features of the FBM, which has been described in detail in Lüdeke et al. (1994). The basic features of the compartment model structure are shown in Fig. 1.

We propose the same basic model structure for every ecosystem type, comprising the presumably minimal subdivision of the total carbon content of the living biomass (**BC**) into 2 compartments (**GC** and **RC**). For simplicity the litter carbon and the humus carbon compartments are considered as one single soil compartment (**SC**).

As shown in Fig. 1 it is assumed that the assimilate production C_{ASS} is specifically dependent on the mass of compartment **GC**. This flux is to be partitioned according to the current needs of the plant organs, namely the build-up and maintenance of the photosynthesizing tissue and of the feeder roots (represented by **GC**) on the one hand, and the build-up and maintenance of stems, branches and coarse roots (represented by **RC**) on the other. Furthermore, assimilates have to be translocated in order to fill particular storage organs, which are included in the carbon mass of the **GC** compartment as well.

The effective carbon assimilation rate, C_{ASS}, is described as a product function of the assimilation capacity α per unit leaf area, the actual leaf area LAI(**GC**) of the canopy, multiplied by a term dependent on light and canopy structure (h_1), a temperature-dependent term (h_2), and a soilwater-dependent term (h_3):

$$C_{ASS} = \alpha \cdot \mathrm{LAI}(\mathbf{GC}) \cdot h_1(I, \mathrm{LAI}(\mathbf{GC})) \cdot h_2(T) \cdot h_3(\mathbf{SW}) \quad (1)$$

The factors h_1, h_2 and h_3 are normalized. Detailed information on the model equations is presented in Appendix Section A1 and Lüdeke et al. (1994).

The dependence on light intensity and leaf area index, LAI, is modeled by the approach of Monsi & Saeki (1953), with LAI = $\frac{1}{2} \cdot \mathrm{SLA} \cdot \mathbf{GC}$, assuming that the leaf carbon mass is half the carbon mass of the **GC** compartment. The conversion factor SLA (specific leaf area) is prescribed for each vegetation type.

The seasonal and long-term patterns of partitioning of the carbon assimilation flux C_{ASS} into the **GC** and **RC** compartments are derived from 2 basic assumptions: (1) the vegetation tends to maximize the amount of

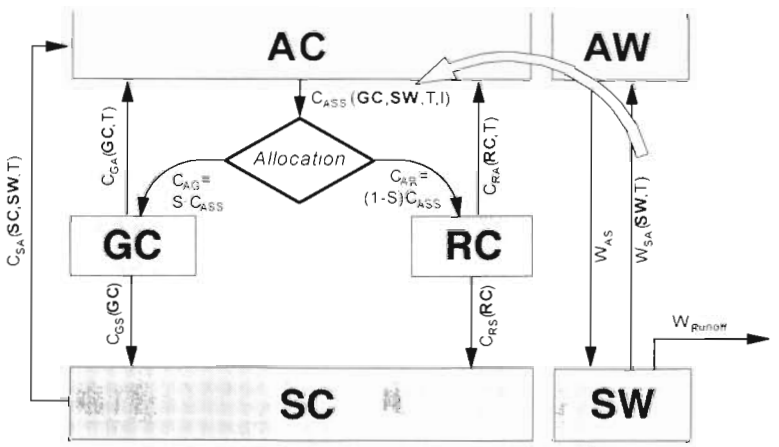

Fig. 1 Flow chart and model structure. Bold capital letters represent the reservoirs of carbon (second letter **C**) and water (second letter **W**): **AC**, atmospheric carbon; **GC**, carbon content of green biomass and feeder root biomass plus assimilate store; **RC**, carbon content of remaining biomass of biota; **SC**, carbon content of litter, humus and dead biomass; **AW**, water in the atmosphere; **SW**, soil water in the rooting zone. Capital letters C and W represent carbon and water fluxes; indices indicate sources and sinks of these fluxes. The functional dependence of the fluxes on the driving variables and pool sizes is given in parentheses (T: air temperature; I: photosynthetically active radiation (PAR)). W_{AS}: precipitation; W_{SA}: actual evapotranspiration. S stands for the fraction of total assimilation, C_{ASS}, that is allocated to **GC**

photosynthesizing tissue (contained in the **GC** compartment); (2) it is possible to identify a function **RC** = Ω(**GC**) that determines the minimum amount of **RC** needed to support and maintain the given amount of **GC**.

Data from field measurements (Reichle 1981) and theoretical considerations suggest that an allometric relationship, expressed here by a fractional power function, is a suitable parameterisation for this partition (see Janecek et al. 1989). In order to comply with the basic assumptions, the system's development within the **GC**-**RC**-phase space is allowed to take place only in the region **RC** $\geq \Omega$(**GC**).

The phenological behaviour of the model is governed by a set of rules for carbon partitioning of evergreen and deciduous vegetation types. Furthermore, we distinguish the following phases:

(i) *a leaf shooting phase:* The carbon gain from photosynthesis is greater than the carbon loss. The system allocates most of the assimilates to the **GC** compartments until the trajectory reaches Ω(**GC**), maximizing its production ability.

(ii) *a secondary growth phase:* The system is forced to allocate simultaneously into the **GC** and **RC** compartments according to the Ω(**GC**) function

$$\mathbf{RC} = \Omega(\mathbf{GC}) = \xi \cdot \mathbf{GC}^{\kappa} \quad (2)$$

where ξ and κ are vegetation-specific parameters.

For the deciduous vegetation within 1 yr (see Fig. 2):

(iiia) *a leaf shedding phase:* At the end of the vegetation period, when unfavourable weather conditions (e.g. drought, cold) do not allow biomass increase, a leaf abscission phase reduces the **GC** compartment to a residual amount of feeder roots and assimilate store, which is proportional to the annual maximum of **GC** and is characterized by the function

$$\mathbf{RC} = \Theta(\mathbf{GC}) = \nu \cdot \mathbf{GC}^{\kappa} \quad (3)$$

with the same exponent κ as in Eq. (2) and a different vegetation-specific parameter ν.

(iv) *a dormancy phase:* When the trajectory reaches the Θ(**GC**) curve the dormancy phase starts. During this phase the biomass losses, as defined by the **RC** respiration and the total litter production, are distributed among the compartments so that the systems trajectory follows the Θ(**GC**) curve. This phase ceases when the weather conditions allow a net biomass increase, assuming a total conversion of stored assimilates into leaf biomass and feeder roots.

For evergreen vegetation only 3 phases are considered, namely leaf shooting, the secondary growth phase and

(iiib) *a standby phase:* The losses of **GC** and **RC** are characterized by constant proportions, until new net growth can be initiated. This phase occurs when the net biomass change is equal to or lower than zero.

The days when the system changes from the dormancy phase (deciduous types) or standby phase (evergreen types), to the leaf shooting phase, and from the secondary growth phase into the leaf shedding or standby phase, are the actual results of the model and are called leaf shooting days and abscission days.

The dynamics of the system for the seasonal and long-term development of a given vegetation type are shown in Fig. 2.

In the FBM seasonal growth is coupled to long-term development of the vegetation. Annual growth occurs in any year in which the annual NPP is larger than the annual litterfall. When this equilibrium is reached, the system performs a 'limit cycle', in which the annual gain in biomass of both **GC** and **RC** is exactly balanced by the litterfall during the less favourable period of the year. We identify this limit cycle with the climax state of a vegetation type for a given set of climatic conditions.

3. DRIVING VARIABLES AND PARAMETERS

The FBM is a general model of vegetation carbon fluxes and balances. For each grid point, calculations are performed depending on the climatic time series for that area, the soil type and the vegetation type. Precipitation is integrated through the water model which is parameterized by a soil-type-dependent available water capacity. Currently, climate is the only input layer that provides time-dependent driving variables. With the climatic values and the soil type assignment, the temporal regime and the abiotic environment for an area of grid elements in the model are determined.

The vegetation map distinguishes 32 vegetation types. There is a characteristic set of parameters associated with each vegetation type. The broadest distinction is made by choosing a different set of equations for carbon allocation within cold-deciduous, drought-deciduous or evergreen vegetation. The selected phenological type and the climate time series are the only information accounting for the seasonal behaviour of a grid element, aside from the structural features of the model described above. Furthermore, each vegetation type is characterized by a set of parameters describing specific temperature dependences of assimilation and respiration fluxes, and another set of parameters representing mean or typical features of the canopy structure and the carbon pool turnover.

As a long-term process model, the FBM imposes no general or explicit restriction on the temporal development of fluxes and pools.

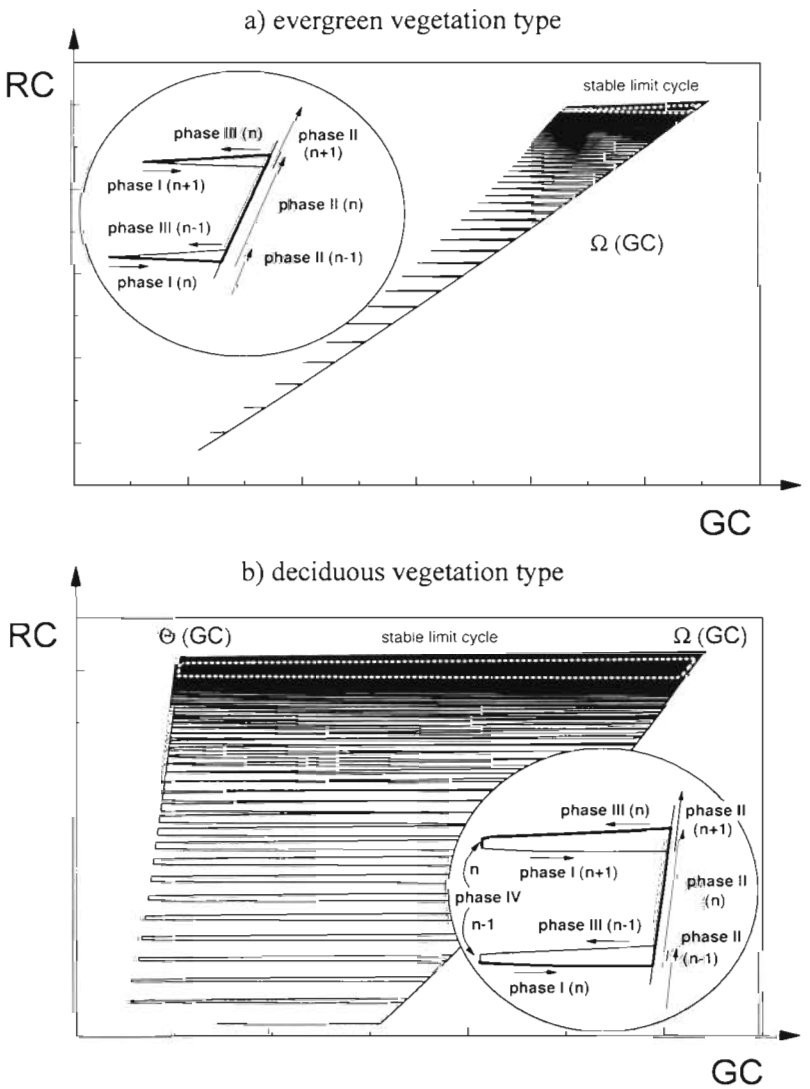

Fig. 2. Phase space representation of (a) an evergreen temperate and boreal forest and (b) a cold-deciduous forest. Started in a non-equilibrium state, the forests reach a stable-limit (equilibrium) cycle after many years. The enlarged inset shows the phases within one particular year n for an intermediate state in long-term development. The dotted lines approximate the stable-limit cycle obtained in the equilibrium state, **Ω(GC)** is the allometric relation between the compartments **RC** and **GC**, and **Θ(GC)** is the minimum amount of **GC** (used as storage)

3.1. Climatic input data

The current version of the FBM uses the CLIMATE database version 2.1 (W. P. Cramer, Potsdam, pers. comm.), which gives monthly values of temperature, precipitation and relative sunshine hours on a 0.5° grid. We interpolate these data to daily values, as described in Lüdeke et al. (1994), and superimpose onto the temperature data a diurnal cycle derived from the daily maxima and minima typical for a particular vegetation type. For simplification, the diurnal cycle is modelled by a cosine function with an amplitude ΔT of 3 to 7°C for the evergreen broad-leaved forests (ranging from 3°C for tropical evergreen to 7°C for temperate evergreen seasonal forests) and 8°C for all other vegetation types, in which the maximum occurs at 14:00 h. Radiation outside the atmosphere is calculated for each time step on the basis of solar geometry (Jones 1992). Cloud and atmosphere attenuation is estimated by the Ångström relationship (Landsberg 1986) using the parameterised form given by A. D. Friend (1995 pers. comm.) as shown in Appendix Section A2.

3.2. Map of hydrological soil properties

The parameters for the water model, i.e. the permanent wilting point (PWP) and the field capacity (FC), were derived for each grid element from the FAO soil map as digitized by Zobler (1986). He distinguished 7 soil texture classes, each characterized by a specific range in the relative content of sand, silt and clay, plus 1 class for organic Θ_{soil} that is associated with 1 of the 7 soil texture classes. For each class the relative or volumetric moisture content soil at PWP and FC was calculated from the soil composition data (see Appendix Section A3).

Typical rooting depths were used to compute the absolute moisture content from the relative moisture content Θ_{soil} and thus provided values of FC and PWP, the difference between which is the available water capacity (AWC). Rooting depth was estimated on a grid element basis from the combination of soil texture and vegetation type as described by Vörösmarty et al. (1989). We chose typical root depths for forest and woodlands to vary from 2.5 m on sandy soils to 1.2 m on clay soils, while for shrublands and grasslands the root depth was chosen to be between 1 m on sandy soils and 0.7 m on clay soils. In addition, following Webb et al. (1993), we limited rooting depth to 5 mm in desert regions and to 10 cm for the tundra. Further details on the estimation of AWC are given in Otto (1997). The resulting global estimates of the soil hydrological properties delimiting the possible range for plant water

uptake are presented in Table 1. As described above, 4 vegetation categories and 7 soil classes are considered.

3.3. Global map of vegetation types

In the well-known vegetation classification of Köppen (1936) the seasonal course of climate variables is used to distinguish broad categories of climate and, with it, typical vegetation. In the Holdrige (1947) life zone concept, mean annual temperature and precipitation variables serve, after the biotemperature is introduced, to describe the different vegetation types. However, biogeochemical models need additional ecological information such as climax biomass and net primary production as initializing conditions, which cannot be computed or correlated by rule-based functions, not even with sophisticated vegetation models such as BIOME 1 (Prentice et al. 1992). Furthermore, for a more detailed description of the vegetation, the climate parameters alone cannot serve to uniquely describe either the standing biomass or the exchange fluxes. Thus it is better to start out with the given classification of the vegetation according to physiognomic and physiological characteristics and then introduce the climate variables afterwards.

This is accomplished in the FBM by creation of a global map of the distribution of 32 vegetation types, which originate from the physiognomic UNESCO classification of 1973 (UNESCO 1973) as re-examined and re-arranged in Matthews' map of potential vegetation of 1983 (Matthews 1983). Table 2 contains an outline of the vegetation types used in FBM 2.0 and 2.1; these are a further modification of Matthews' vegetation types, with the main distinction being the introduction of C_3- and C_4-dominated grassland ecosystems.

Within the classification a distinction is made between forest and woodland ecosystems, where woodlands have a projected leaf cover between 10 and 30%. Shrubland ecosystems including the tundra are the third category, with the shrub height extending up to 4 m. The fourth category comprises grassland ecosystems, which are subdivided into the large groups of savannas in the tropical climate belt and steppes or prairies in the temperate zone.

A disaggregation of grassland vegetation types was necessary because the characteristic climates were too different. In the present study we consider 4 grassland types in the tropics (vegetation types 30 to 33) and 4 grassland types in the temperate zone (vegetation types 34 to 37) All tropical grasslands are dominated by C_4 grasses, while for the temperate grasslands a distinction was made between the 2 types C_3 and C_4 using a temperature criterion (C_4-dominated grasslands require the temperature of the warmest month to be $\geq 22°C$, and of the coldest month $\geq -1°C$).

For ease of associating the different ecosystems with specific parameters or simulation results we introduced a 5-letter code for each ecosystem. With the first letter we distinguish the 4 principal ecosystem types: forests, woodlands, shrublands and grasslands. The second letter characterizes 3 temperature regimes, hot, temperate and cold, while the third letter describes the soil moisture classes moist, intermediate, dry and seasonal, the last category chosen where there are extended rainy and dry periods. The fourth letter describes the leaf type, where a distinction is made between broad- and needle-leaved plants, plants with xeromorphic leaves, and C_3 and C_4 grasses. The mixed category of the tundra with grasses and broad-leaved shrubs is simply classed as tundra, while forests may also show an association of needle- and broad-leaved types. Finally the fifth letter refers to the longevity of the leaves, whereby the cold-deciduous and drought-deciduous types shed their leaves every year in contrast to the evergreens which do not.

In Fig. 3 we present the vegetation map used in the FBM. Extreme deserts and ice-covered land appear as brown and blue areas, for which no calculations are performed.

Table 1 Field capacity (FC) and available water content (AWC, in parentheses), given in mm, for different soil-vegetation combinations based on Zobler (1986) soil textures and the FBM vegetation-type classifications as used within the soil water model

Vegetation category	Zobler soil texture:						
	Coarse	Coarse + medium	Medium	Coarse + fine	Coarse + medium + fine	Fine	Medium + fine
Forest and woodland	375.8 (213.7)	522.7 (264.3)	545.2 (274.8)	538.9 (204.4)	537.4 (226.0)	654.1 (189.4)	527.6 (203.1)
Grass- and shrubland	187.9 (106.8)	261.4 (132.2)	340.8 (171.7)	336.8 (127.8)	– –	381.6 (110.5)	307.7 (118.5)
Tundra	18.8 (10.7)	26.1 (13.2)	34.2 (17.2)	33.7 (12.8)	33.6 (14.1)	54.5 (15.8)	44.0 (16.9)
Xerophytic shrubland	187.9 (118.4)	261.4 (147.9)	340.8 (192.2)	– –	– –	381.6 (127.0)	307.7 (134.7)

Table 2. Vegetation types used in the FBM based on Matthews' (1983) vegetation types, modified considering data of Schmithüsen (1976)

Forest ecosystems		
1	FHMBE	Tropical evergreen forest, mangrove forest
2.	FHSBE	Tropical/subtropical evergreen seasonal broad-leaved forest
3.	FHIBE	Subtropical evergreen rainforest
4.	FTMBE	Temperate/subpolar evergreen rainforest
5.	FTSBE	Temperate evergreen seasonal broad-leaved forest, summer rain
6.	FTSXE	Evergreen broad-leaved sclerophyllous forest, winter rain
7.	FHSNE	Tropical/subtropical evergreen needle-leaved forest
8.	FCDNE	Temperate/subpolar evergreen needle-leaved forest
9.	FHSBD	Tropical/subtropical drought-deciduous forest
10.	FTMAC	Cold-deciduous forest, with evergreens
11	FCSAC	Cold-deciduous forest, without evergreens
Woodland ecosystems		
12.	WHSXD	Xeromorphic forest/woodland
13.	WHSBE	Evergreen broad-leaved sclerophyllous woodland
14.	WCDNE	Evergreen needle-leaved woodland
15.	WHSBD	Tropical/subtropical drought-deciduous woodland
16.	WCDNC	Cold-deciduous woodland
Shrubland ecosystems including tundra		
20.	STDBE	Evergreen broad-leaved shrubland/thicket, dwarf-shrubland
21.	SCDNE	Evergreen needle-leaved/microphyllous shrubland/thicket
22.	STDBD	Drought-deciduous shrubland/thicket
23.	SCDBC	Cold-deciduous subalpine/subpolar shrubland,dwarf shrubland
24.	SHSXE	Tropical xeromorphic shrubland/dwarf shrubland
25.	STDXD	Temperate dwarf shrubland
26.	SHDXE	Tropical dry xeromorphic shrubland/dwarf shrubland
27.	SCDTC	Arctic/alpine tundra, mossy bog
Grassland ecosystems		
30.	GHM4E	Tropical grassland (C4) with woody tree cover/humid savanna
31.	GHS4D	Tropical grassland (C4)/dry savanna
32.	GHD4E	Tropical grassland (C4)/thorn savanna
33.	GHD4D	Tropical grassland (C4)/small-leaved thorn-tree woodland
34.	GTM3D	Temperate grassland (C3) with woody tree cover
35.	GTM4D	Temperate grassland (C4) with woody tree cover
36.	GTD3D	Temperate grassland (C3)/steppe, prairie
37.	GTD4D	Temperate grassland (C4)/steppe, prairie

Legend for the 5-letter code:

1st letter, ecosystem	2nd letter, temperature	3rd letter, moisture	4th letter, leaf type	5th letter, leaf longevity
F forest	H hot	M moist	B broad-leaved	C cold-deciduous
W woodland	T temperate	I intermediate	N needle-leaved	D drought-deciduous
S shrubland	C cold	D dry	X xeromorphic	E evergreen
G grassland		S seasonal	T tundra	
			A association of needle- and broad-leaved	
			3 C3 grass	
			4 C4 grass	

3.4. Ecological and ecophysiological estimates and parameters

3.4.1. Characterization of vegetation types

Each vegetation type is characterized by its plant-phenological and its associated soil-heterotrophic-respiration type and by a specific set of model parameters that are estimated based on data from various sources or derived from ecological estimates through an equilibrium calibration procedure. The estimates and parameters for all vegetation types are listed in Table A2 of the Appendix.

In the model, 3 phenological types are distinguished by different sets of possible phenophases or leaf abscission rules. The last letter of the 5-letter code identifies a vegetation type as cold-deciduous (C), drought-deciduous (D) or evergreen (E). The respira-

tion group (RG = 1, ..., 4) determines the equations used to calculate the temperature response of heterotrophic respiration (after Fung et al. 1987) (see Table A3 in the Appendix).

Table A3 gives the ecophysiological parameters determining the temperature dependence of assimilation and autotrophic respiration, the parameters determining the limiting curves in the **GC**-**RC**-phase space and the specific conversion factors used to calculate LAI and the respiration group.

The 3 temperature parameters T_{min}, T_{max} and T_{opt} (minimum, maximum and optimum temperature; adapted from Larcher 1984) determine the temperature response of net photosynthesis, while ω describes the temperature dependence of respiration (derived from Ryan 1991).

The allometric relationships in Eqs. (2) & (3) are characterized by the parameters κ, ξ, and ν. The exponent κ was derived from biomass data by curve fitting (Janecek et al. 1989). The parameters ξ and ν were calculated from ecological estimates listed in Table A4 With the assumption of $\mathbf{RC}_{max} = \Omega(\mathbf{GC}_{max})$ it follows that:

$$\xi = \mathbf{RC}_{max} \cdot \mathbf{GC}_{max}^{-\kappa} \tag{4}$$

For deciduous vegetation types, where litter production from **GC** is concentrated in the leaf shedding phase at the end of the growing season, the annual net input into the **GC** compartment, NPP_G, can never be larger than the maximum size of that compartment, $\mathbf{GC}_{max}$. After leaf abscission a certain fraction of **GC**, namely $(\mathbf{GC}_{max} - NPP_G)/\mathbf{GC}_{max}$ is kept in the plants' assimilate stores. This fraction, which determines ν in the allometric relation was found to vary over the deciduous vegetation types between 15 and 65%, consistent with ecological expectations. In analogy to the derivation of ξ we calculate the parameter ν:

$$\nu = \mathbf{RC}_{max} \cdot (\mathbf{GC}_{max} - LpG)^{-\kappa} = \xi \cdot \left(\frac{\mathbf{GC}_{max} - NPP_G}{\mathbf{GC}_{max}} \right)^{-\kappa} \tag{5}$$

where LpG is litter production in the **GC** compartment. From the magnitude of the **GC** compartment and the specific leaf area estimated for each vegetation type (Lüdeke et al. 1994), the leaf area index can be calculated:

$$LAI = SLA \cdot \mathbf{GC}/2 \tag{6}$$

noting that **GC** is subdivided into 2 equal parts, namely leaves and fine roots.

The calibrated parameters are based on estimates of the maximum compartment size at climax for the 3 state variables **GC**, **RC** and **SC**. Furthermore, the annual integrals of carbon fluxes are needed. Under equilibrium conditions the annual integrals of 4 fluxes are sufficient for the description of all annual flux balances in the model, because NPP equals litter production as well as heterotrophic respiration. Bearing in mind that there is no material exchange between the **GC** and **RC** compartments, we can write

$$NPP_G = GPP_G - ResG = LpG \tag{7}$$

and

$$NPP_R = GPP_R - ResR = LpR \tag{8}$$

as well as

$$RES = NPP = LpG + LpR \tag{9}$$

where GPP_X, ResX and LpX denote the annual integrals of the photosynthetic uptake fluxes C_{AX}, the autotrophic respiration fluxes C_{XA} and the litter production C_{XS} for the 2 biotic compartments (X = G or R) and RES denotes the annual integral of heterotrophic respiration.

In Appendix Section A5 we show that the ecological data for forests and woodlands suggest that the litter production ratio LpG/LpR equals ca 1 at the climax state. Within the 32 vegetation types considered in this study all but 3 grassland types were assigned this ratio, while grassland type 30/GHM4E was assigned the ratio 2:1 and grassland types 36/GTD3D and 37/GTD4D the ratio 9:10 (see below).

Similarily, as ecological data suggested that autotrophic respiration from the **GC** and **RC** compartments of a given vegetation type are approximately equal, we set the ratio ResG/ResR equal to 1 for all types:

$$ResG = ResR \tag{10}$$

From the relations above it follows that the estimated ratios for NPP_G/NPP_R and GPP_G/GPP_R are equal to 1 for all but the 3 grassland vegetation types mentioned. The annual flux of gross assimilation can also be calculated. GPP = NPP + 2ResG. From the 3 flux integral estimates presented in Table A2 for each vegetation type, together with Eqs. (7) to (9) and the assumption of ResG = ResR, all 7 annual flux integrals for an equilibrium run can be determined.

Our estimates of mean values of climax biomass and net primary productivity are based on parameter values as given by Matthews (1984) and Fung et al. (1987) respectively for the vegetation types of Matthews' original map (1983). The ratios of maximum annual pool sizes ($\mathbf{GC}_{max}/\mathbf{RC}_{max}$), the GPP/NPP ratios—determining autotrophic respiration—and values for the organic soil carbon content were derived from various sources (see Lüdeke et al. 1994 for details).

In Table A3 we list the estimates of carbon pools and fluxes for all vegetation types. Because of the equilibrium state condition and the adopted symmetry in the autotrophic respiration fluxes for the compartments **GC** and **RC**, only NPP and the annual fluxes for respiration and litter production from the **GC** compartment, ResG and LpG, are given in the table.

Along with the division of grasslands and in order to examine how much the LpG/LpR ratio of non-woody vegetation types deviated from the value derived for forests and woodlands, a new data set of ecological parameters had to be constructed for grassland biomes. Using the data of Coupland (1979) for 11 different North American sites of the vegetation type 'temperate grassland/steppe, prairie' (vegetation types 36/GTD3D and 37/GTD4D), we obtained typical values for the mean biomass and annual production of the plant organs green shoots, roots and crowns as well as the mean biomass of dead shoots. These data could be rearranged to fit our model requirements to determine the climax values of $\mathbf{GC}_{max}$ (0.28 kg C m^{-2}) and $\mathbf{RC}_{max}$ (0.65 kg C m^{-2}) as well as the annual litter production of **GC** (LpG = 0.18 kg C m^{-2} yr^{-1}) and of **RC** (LpR = 0.20 kg C m^{-2} yr^{-1}). It is interesting to note that even for the grasslands in the temperate zone the litter production from both compartments is nearly in the ratio of 1:1.

For the vegetation type 'temperate grassland with woody tree cover' (vegetation types 34/GTM3D and 35/GTM4D) we obtained the respective ecological parameters by averaging the above-determined biomass and fluxes with the values for the vegetation type 'cold-deciduous woodland' (vegetation type 16/WCDNC).

For the tropical grasslands we used the database of Rodin & Bazilevich (1968) and Coupland (1979). Here we assigned to the vegetation type 'humid savanna' (type 30/GHM4E) a NPP of 0.9 kg C m^{-2} yr^{-1}, of which 0.6 kg C m^{-2} yr^{-1} is allocated to the **GC** compartment. With the $\mathbf{GC}_{max}$ biomass of 0.3 kg C m^{-2} a rapid mean turnover of the herbaceous tissue of half a year results. The same data sources show for the 'dry savanna' (type 31/GHS4D) a turnover of approximately 1 yr and a NPP value of 0.4 kg C m^{-2} yr^{-1}.

In Lüdeke et al. (1994) we examined temperate/subpolar evergreen needle-leaved forests (vegetation type 8/FCDNE) using as ecological parameters a mean climax biomass of 13.42 kg C m^{-2} (according to Matthews 1984) and an annual NPP of 0.585 kg C m^{-2} yr^{-1} (according to Fung et al. 1987). Since these values are similar to the suggested parameter values for temperate deciduous and mixed forests (vegetation types 10/FTMAC and 11/FCSAC), simulation of the NPP for the northern biomes resulted in the contradiction that several northern regions covered by boreal forests showed higher NPP values than the neighbouring areas covered with vegetation type 10 or 11 in lower latitudes. Following the current debate with respect to estimates of biomass density and NPP in boreal forests (Wisniewski & Sampson 1993) it was considered reasonable to determine new ecological parameter values for vegetation type 8 based on recent estimates. Apps et al. (1993) compiled estimates of biomass for several regions covered by boreal forests. These estimates range from 2.63 to 8.33 kg C m^{-2} with an average of 5.12 kg C m^{-2}. Kolchugina & Vinson (1993) estimate an average NPP of 310 g C m^{-2} yr^{-1} for the forests of the former Soviet Union. Viereck et al. (1983) reported measurements of aboveground NPP for different tree species in less productive Alaskan regions of the boreal zone. They amounted to 55 g C m^{-2} yr^{-1} for black spruce (*Picea mariana*) and 180 g C m^{-2} yr^{-1} for white spruce (*Picea glauca*). Accordingly we introduced a new estimate of 6.75 kg C m^{-2} for the biomass in the climax state—amounting to half of the value originally presented by Matthews (1984)—and adopted the NPP value of 310 g C m^{-2} yr^{-1} from Kolchugina & Vinson (1993), which is also approximately half of the estimate given by Fung et al. (1987).

The reevaluation of LpG/LpR ratios and equilibrium turnover times of carbon pools led us to adopt higher estimates of the biomass target values of the deciduous forests (vegetation types 9 to 11, FHSBD, FTMAC, FCSAC). For example, for vegetation type 11/FCSAC the total biomass at equilibrium had to be increased from 12.6 kg C m^{-2} to 16.2 kg C m^{-2}.

The mean carbon pool turnover times in the equilibrium state are defined as the ratio of the state variables at climax ($\mathbf{GC}_{max}$, $\mathbf{RC}_{max}$ and $\mathbf{SC}_{max}$) to the annual fluxes of NPP or the corresponding litter production Lp. In Table 3 the residence times for the compartments **GC**, **RC** and **SC** resulting from the ecological estimates as given in Table A3 are shown. For deciduous vegetation types the residence time of **GC** is 1 growing season, formally set equal to 1 in the table. For the evergreen vegetation $\tau(\mathbf{GC})$ is ≥ 1 yr, as is to be expected. The residence times $\tau(\mathbf{RC})$ range from 3.6 to 58.8 yr, being largest for the forests, smaller for woodlands and shrublands and, in general, still smaller for grasslands. The short turnover times for the soil are caused by modelling the soil as a single compartment. If litter and humus compartment is distinguished, where only a fraction of 5 to 25% is converted to humus, the residence times increase substantially. As the fluxes to the humus compartment are reduced by the same proportion, the soil residence times become larger by a factor of 4 to 20.

In Table 3 we have defined the turnover times with respect to NPP and Lp. Alternatively, we could have chosen the gross primary production or the corresponding sum of litter production and autotrophic respiration as the characteristic fluxes. However, since the residence times for assimilates used in respiration are very short compared to those of the structural material, we have chosen not to incorporate GPP in the residence time calculations.

Table 3. Residence time of carbon in the 3 compartments for all vegetation types (VT) using their typical parameter set. Typical τ(**SC**) values are rather low because no distinction is made between the litter and the soil humus compartment. (For explanation of the 5 letter code of the vegetation types see Table 2)

VT	Code	τ(**GC**) (yr)	τ(**RC**) (yr)	τ(**SC**) (yr)
1.	FHMBE	1.7	41.1	11.6
2.	FHSBE	2.0	37.4	12.5
3.	FHIBE	2.0	37.4	12.5
4.	FTMBE	1.0	25.0	18.4
5.	FTSBE	1.0	25.0	18.4
6.	FTSXE	2.3	42.7	40.0
7	FHSNE	3.9	39.0	17.5
8.	FCDNE	5.4	47.6	45.2
9.	FHSBD	1	28.8	18.0
10.	FTMAC	1	58.8	22.2
11	FCSAC	1	58.8	22.2
12.	WHSXD	1	14.2	14.0
13.	WHSBE	2.1	27.9	22.2
14.	WCDNE	6.2	32.4	25.7
15.	WHSBD	1	27.6	21.7
16.	WCDNC	1	28.2	22.2
20.	STDBE	1.5	17.1	24.1
21	SCDNE	1.6	25.4	50.0
22.	STDBD	1	16.8	16.7
23.	SCDBC	1	16.9	23.6
24.	SHSXE	1.6	11.7	33.3
25.	STDXD	1	5.3	16.7
26.	SHDXE	1.0	6.2	50.0
27	SCDTC	1	7.0	190.0
30.	GHM4E	0.5	10.0	6.7
31.	GHS4D	1	4.5	13.8
32.	GHD4E	2.0	16.0	40.0
33.	GHD4D	1	5.3	33.3
34.	GTM3D	1	15.1	16.2
35.	GTM4D	1	15.1	16.2
36.	GTD3D	1	3.3	31.6
37.	GTD4D	1	3.3	31.6

3.4.2. Calibration

It should be noted that the ecological estimates and assumptions referring to carbon pool and flux integral sizes presented in Table A3 enter only into the calibration process, in which a characteristic climate is used to evaluate the rate parameters for photosynthesis, respiration and litter fall as given in Table A4. For any individual grid element within a vegetation type, the annual course of all fluxes and pool sizes and, by that, the annual integrals are calculated independently as driven by local climate, and they differ from the mean ecological estimates as much as the climatic input differs from the characteristic climate.

In Lüdeke et al. (1994) we described in detail the procedure of finding the characteristic climate associated with each vegetation type. Essentially, the procedure consists of a linear superimposition of the course of the climate variables on each of the grid elements with a phase shift such that the maxima in the annual course of temperature, precipitation and radiation are conserved.

A numerical calibration procedure is then used to determine the 6 free parameters of the model equations for carbon uptake and release. The resulting parameter sets for all vegetation types are given in Table A4. With these parameters, an equilibrium model run driven by the characteristic climate for a certain vegetation type reproduces the annual fluxes and the maximum pool sizes at the equilibrium state estimated for that type, as given in Table A3. A typical phenology in terms of the date of the year when phase transitions occur also results from the calibration run for each vegetation type but is not used in parameterisation of the model equations.

We decided to calibrate the model using typical climate input and ecological target values representing the conditions for a given vegetation type instead of arbitrarily chosen calibration sites, in order to prevent specific sets of local variables from gaining too much weight within the global model, which could not be justified. Furthermore, this approach provides a general interface between ecological measurements and model calibration that does not depend on a scientific decision of what is typical for a given type of vegetation, and it is suitable for incorporating increasing numbers of ecological measurements from all over the world in a well-defined way. Structurally, however, there would be no difference in calibrating the model using site data.

However, for some vegetation types the average annual NPP of all grid elements characterized by their individual climate deviated from the corresponding target value. In these cases a second calibration set was introduced, in which for simplicity only the most sensitive parameter with respect to assimilation was changed, namely α. This deviation results from the fact that the climate variables enter in a non-linear way into the carbon assimilation flux C_{ASS} and its allocation.

4. RESULTS OF SIMULATIONS

4.1. Regional distribution of NPP and LAI_{max}

4.1.1. Net primary productivity

Using the long-term climate data and the potential vegetation map described above the FBM estimates the global annual NPP to be 50.28 Gt C The regional distribution of NPP as shown in Fig. 4 reflects on the one hand the distribution of the vegetation types and

on the other the spatial variability in climate and soil within each vegetation type.

Looking at the different vegetation types the highest NPP values occur in the tropical zones ranging from 0.34 to 1.44 kg C m^{-2} yr^{-1} in the evergreen rainforest (type 1/FHMBE). The lowest values occur in hot and dry or very cold regions; e.g. for the tundra ecosystems the FBM predicts a NPP between 0 and 0.2 kg C m^{-2} yr^{-1}.

In Fig. 5 the regional distribution of the NPP *within* several vegetation types is shown. Due to the climatic gradients the model simulates a broad variety of NPP values. Nevertheless it can be seen with reference to Table A3 that the simulated average NPP for each vegetation type meets the target value fairly well. In general the target value coincides with the maximum of the distribution.

Especially forest ecosystems such as the tropical and temperate forests match a bell-shaped Gaussian-type or a skewed Poisson distribution quite well. The cal-culations for the tropical evergreen forest (vegetation type 1/FHMBE) result in a mean annual NPP of 0.985 kg C m^{-2} yr^{-1} (standard deviation σ = 0.148 kg C m^{-2} yr^{-1}), while the target value amounts to 0.945 kg C m^{-2} yr^{-1}. The mean NPP for the boreal forests is calculated to be 0.331 kg C m^{-2} yr^{-1} (σ = 0.081 kg C m^{-2} yr^{-1}) compared with the target value of 0.310 kg C m^{-2} yr^{-1}. A fraction (2.4%) of the boreal forest area shows a calculated NPP less than 0.06 kg C m^{-2} yr^{-1}. These areas are located in the northernmost parts of the vegetation type with extreme low temperatures. The calculated values of NPP are of course too small to be realistic either for the boreal forests or the adjoining tundra, indicating a probable mismatch between the vegetation map and the climate map.

In the case of the cold-deciduous forest with evergreens (vegetation type 10/FTMAC) as well, a far extension into the northern regions leads to a relatively high percentage of area related to the lower NPP classes. The calculated mean value for NPP amounts to 0.559 kg C m^{-2} yr^{-1} (σ = 0.146 kg C m^{-2} yr^{-1}), while according to the target value a mean NPP of 0.540 kg C m^{-2} yr^{-1} should be achieved. In contrast to the cold-deciduous forest, the NPP values for tropical drought-deciduous forest (vegetation type 9/FHSBD) follow a bell-shaped distribution with a mean value of 0.573 kg C m^{-2} yr^{-1} compared with a target value of 0.555 kg C m^{-2} yr^{-1} (σ = 0.192 kg C m^{-2} yr^{-1}).

Considering the NPP distribution of the tundra (vegetation type 27/SCDTC) it should be mentioned that this is a vegetation type consisting of dwarf trees, shrubs, grasses, mosses and lichens extending far to the north. Therefore, Walter & Breckle (1986) subdivided the biome tundra into arctic desert, northern and southern tundra and forest tundra. From south to north the vegetation cover decreases from 100% in the southern tundra to isolated, widely scattered cushions in the arctic desert. Estimates of NPP in tundra ecosystems range from 0.0036 kg C m^{-2} yr^{-1} in the arctic desert to 0.35 kg C m^{-2} yr^{-1} in the forest tundra (Wielgolaski et al. 1981). The calculated NPP values lie in this range, but a large part of the total area has a NPP less than 0.065 kg C m^{-2} yr^{-1} as expected from the characteristics of the tundra biome. The mean NPP amounts to 0.088 kg C m^{-2} yr^{-1} (σ = 0.05 kg C m^{-2} yr^{-1}) compared to the target value of 0.100 kg C m^{-2} yr^{-1}.

For temperate grassland with tree cover (vegetation type 34/GTM3D) the target value of 0.370 kg C m^{-2} yr^{-1} is reproduced fairly well by the simulated mean NPP of 0.376 kg C m^{-2} yr^{-1} (σ = 0.164 kg C m^{-2} yr^{-1}). Small deviations from the target NPP value of any particular vegetation type arise from the fact that an individual grid element with a mean temperature and precipitation deviating from the typical climate responds in a non-linear way to the climate variations.

4.1.2. Leaf area index

Because of the linear relationship (Eq. 6) between **GC** and LAI, the leaf area index can be easily evaluated for every day of the year. In Fig. 6 LAI_{max} is shown. Analogously to the NPP map (Fig. 4) the map of maximum LAI reflects the distribution of the vegetation types as well as the climatic gradients within each vegetation type.

The highest maximum LAI values are simulated for evergreen rainforest vegetation type 1/FHMBE (range 4 to 11, average 8.5); the lowest ones are found in the vegetation types 21 (evergreen needle-leaved/microphyllous shrubland/thicket), 24 (tropical xeromorphic shrubland/dwarf shrubland), 25 (temperate dwarf shrubland), and 32 (tropical grassland (C_4)/thorn savanna). In these vegetation types most grid elements have a LAI below 1.

It should be emphasized that in the FBM the size of the compartments is calculated following mechanistic rules. The calculated LAI can be used in comparisons with diagnostic models, which deduce LAI from the NDVI (Lüdeke et al. 1996).

4.2. Seasonal course of simulation results

The capability of the FBM to simulate the seasonality of the terrestrial vegetation is illustrated in Figs. 7 & 8. In agreement with international nomenclature we represent the monthly values of the carbon fluxes with the same symbols used conventionally by ecologists for the

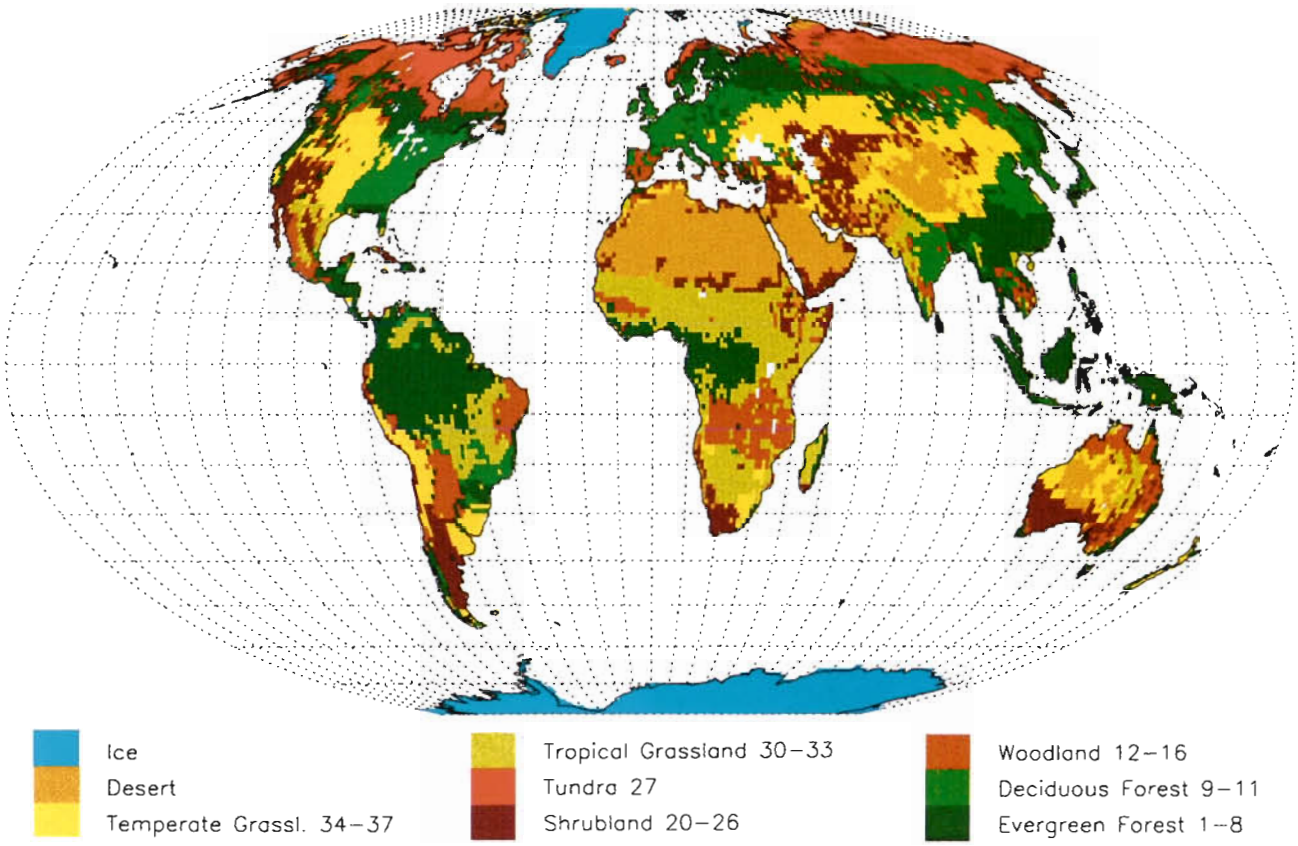

Fig. 3. Vegetation map used in FBM [based on Matthews' (1983) vegetation types, modified considering data of Schmithüsen (1976)]

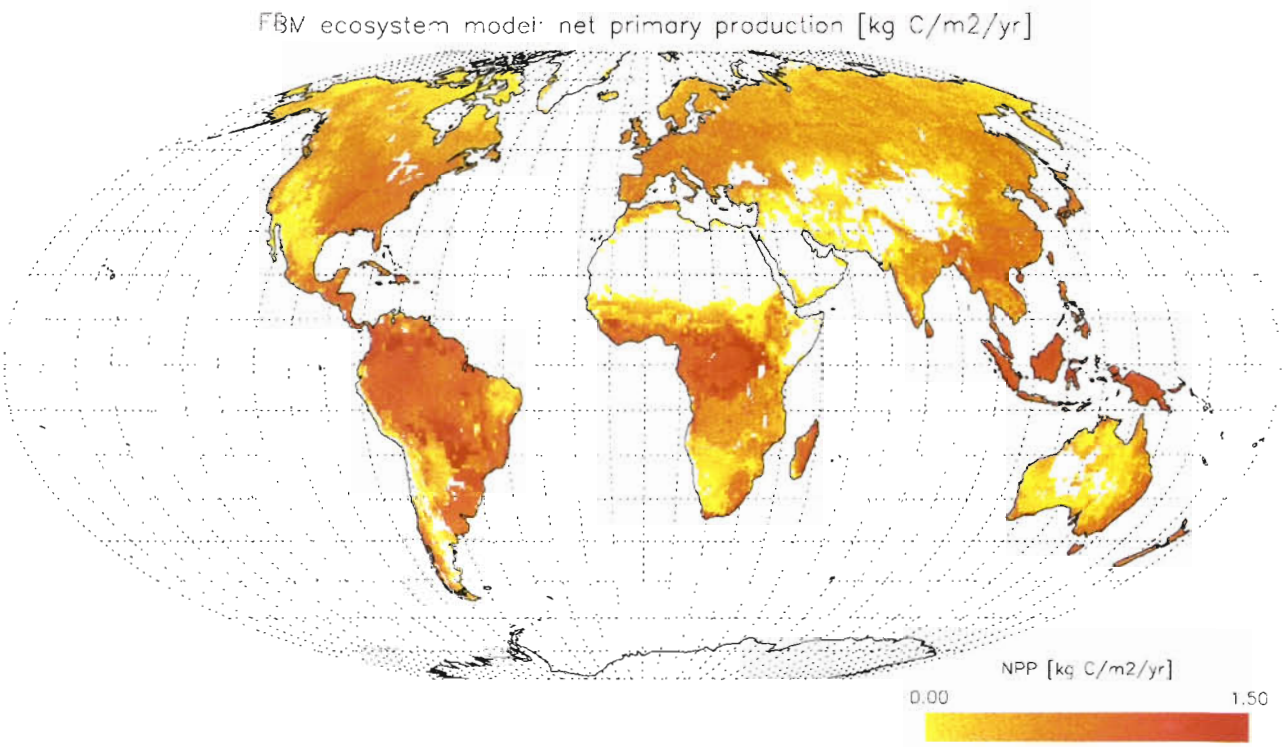

Fig. 4. Annual values of the global net primary productivity (NPP, kg C m^{-2} yr^{-1}) simulated with the FBM. In the simulation run an equilibrium state of the vegetation is assumed. In the map the non-coloured regions correspond to the land-surface types desert and ice, which are not taken into consideration in the simulation, and to non-converging grid elements (~5% of the vegetated area)

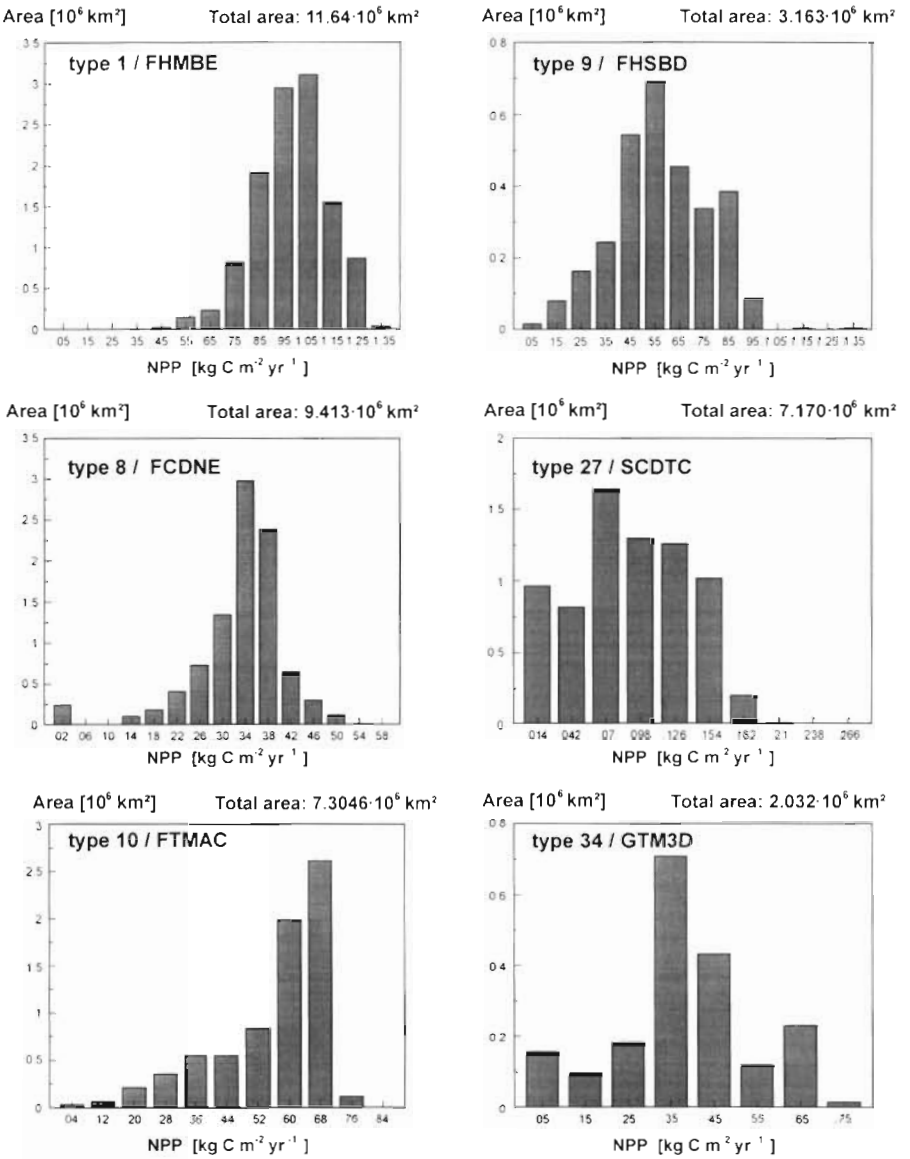

Fig. 5. Area-related NPP distribution for selected vegetation types (see Table 2 for vegetation type descriptions)

annual integrals, i.e. net assimilation as NPP, heterotrophic respiration as RES, and net ecosystem production as NEP. In our model NPP is always calculated as gross primary productivity minus autotrophic respiration. Therefore monthly NPP may be slightly negative during periods of unfavourable environmental conditions, though the annual NPP has a positive value.

4.2.1. North-south transect

As an illustration of the regional fluxes predicted by the FBM we show, in Fig. 7, NPP, RES and the resulting NEP along the transect at 30° E extending from northern Russia to South Africa. From north to south the first 3 selected grid elements, which belong to the same vegetation type (type 8/FCDNE), show a decline in the amplitude and a shift of the maximum towards the beginning of the year in all 3 fluxes and an elongation of the vegetation period, which may be defined as the period when gross primary productivity exceeds autotrophic respiration (NPP > 0). This pattern clearly follows the north-south gradient of local climate, with increasing temperature and precipitation. North of the Black Sea (Ukraine) and in Turkey, low precipitation results in shorter vegetation periods, but at the southern rim of the Sahara desert (Sudan) seasonality can

Table 4. Vegetation-covered area (deserts and ice deserts excluded), number of 0.5° × 0.5° grid elements with vegetation cover and monthly values of NPP in latitudinal belts of 5° width. The last column gives the annual values of NPP in the latitudinal belts (sum of 12 monthly values). The last row gives the global sum over all latitudes. Totals may not add exactly due to rounding

Belt (° lat.)	Belt area (10^3 km^2)	Pixels (0.5°×0.5°)	Monthly values of NPP (Mt C mo^{-1} belt^{-1}) Jan	Feb	Mar	Apr	May	Jun	Jul	Aug	Sep	Oct	Nov	Dec	Total (Mt C yr^{-1})
80.0 to 75.0	21.14	30	−0.02	−0.02	−0.03	−0.03	−0.05	0.24	0.60	0.26	−0.05	−0.05	−0.03	−0.03	0.79
75.0 to 70.0	1493.56	1532	−3.67	−3.44	−4.39	−5.69	−5.67	58.22	96.15	43.18	−3.81	−8.90	−5.02	−4.20	152.76
70.0 to 65.0	5521.84	4629	−19.22	−18.14	−25.08	−19.14	70.85	361.96	432.09	255.22	50.21	−33.69	−27.56	−22.02	1005.49
65.0 to 60.0	6748.50	4738	−36.10	−35.13	−44.90	28.49	259.31	526.97	587.94	424.47	178.68	−20.65	−48.81	−41.13	1779.13
60.0 to 55.0	6343.42	3816	−41.56	−39.79	−51.12	36.45	324.79	565.56	641.78	532.16	296.26	24.92	−59.76	−48.69	2181.01
55.0 to 50.0	7869.97	4176	−64.90	−60.35	−76.70	33.36	509.97	875.41	917.70	756.58	465.09	52.93	−86.82	−77.93	3244.35
50.0 to 45.0	8045.46	3855	−70.82	−64.29	−77.10	74.22	524.38	849.94	911.50	701.76	483.08	139.72	−66.11	−81.44	3324.83
45.0 to 40.0	6283.48	2760	−49.19	−41.46	−44.39	80.50	408.54	690.44	708.93	506.65	392.35	220.06	−2.32	−50.22	2819.90
40.0 to 35.0	5591.95	2278	−21.13	−6.96	13.85	115.49	327.75	472.40	449.92	357.97	290.15	192.37	41.41	−16.83	2216.38
35.0 to 30.0	4914.55	1886	−1.17	15.37	48.59	113.68	227.80	299.32	319.91	292.54	240.14	195.09	67.00	0.65	1818.90
30.0 to 25.0	3693.19	1346	62.43	77.00	126.22	147.25	171.05	152.84	144.84	152.03	151.78	161.16	121.72	69.96	1538.28
25.0 to 20.0	2946.38	1032	128.03	102.31	43.57	−6.30	37.86	91.11	158.21	216.67	249.60	269.92	218.64	160.84	1670.46
20.0 to 15.0	2523.10	855	118.55	42.36	−43.68	−85.29	−15.09	75.05	146.69	191.32	207.56	236.77	218.35	175.02	1267.61
15.0 to 10.0	4076.72	1349	42.07	−17.80	−70.66	−80.08	−16.91	71.62	163.44	254.03	301.47	309.98	175.80	93.75	1226.73
10.0 to 5.0	4797.15	1564	127.10	−11.98	−15.26	110.92	267.50	351.56	421.53	466.41	472.75	494.18	431.90	308.99	3425.60
5.0 to 0.0	4275.08	1383	309.75	263.77	316.47	371.53	411.06	409.11	435.94	436.16	410.68	367.07	323.74	336.12	4391.40
0.0 to −5.0	5134.04	1661	476.58	466.64	498.66	474.85	477.80	452.41	422.48	315.11	222.16	247.84	304.71	387.31	4746.56
−5.0 to −10.0	4896.37	1596	439.29	416.23	456.67	442.17	451.22	347.66	193.33	−5.59	−1.71	180.14	308.28	378.88	3606.56
−10.0 to −15.0	4233.58	1402	403.81	391.56	411.75	376.15	331.07	226.05	119.90	−20.59	−75.54	30.17	172.69	328.75	2695.76
−15.0 to −20.0	4724.97	1601	335.16	390.21	436.02	374.06	284.36	177.95	118.78	47.20	−13.77	5.90	63.43	192.86	2412.16
−20.0 to −25.0	4135.14	1446	168.18	223.46	254.20	211.45	165.13	113.23	97.87	82.65	34.99	21.52	32.85	79.51	1485.05
−25.0 to −30.0	3315.53	1208	149.50	145.05	140.12	109.66	66.11	29.35	31.60	46.07	51.48	82.72	107.81	133.42	1092.89
−30.0 to −35.0	2804.34	1071	192.69	150.16	130.92	87.47	13.86	−1.09	6.40	22.62	45.13	131.16	184.53	220.63	1184.49
−35.0 to −40.0	982.80	399	112.32	71.41	57.05	29.47	−12.33	−12.64	−9.45	−0.65	25.00	69.60	109.40	134.95	574.13
−40.0 to −45.0	432.63	189	55.71	40.23	30.02	11.08	−3.77	−7.92	−5.87	−0.48	8.37	23.66	40.37	55.28	246.67
−45.0 to −50.0	229.36	109	26.54	20.18	14.95	5.78	−1.58	−4.10	−3.12	−0.70	2.53	9.03	16.81	24.48	110.80
−50.0 to −55.0	165.26	88	16.82	12.90	8.99	2.28	−2.07	−2.81	−2.47	−1.30	0.22	4.82	9.53	14.87	61.79
Total	106199.50	47999	2856.76	2529.47	2534.75	3039.77	5272.95	7169.83	7506.63	6071.75	4484.80	3407.44	2652.54	2753.77	50280.46

hardly be recognized. When crossing the equator (Zaire and Burundi) a 6 mo shift is evident in the biospheric fluxes. Further south in regions with woodland and grassland vegetation, the strong seasonality in precipitation, with a maximum total amount of 125 mm from May to October, and larger annual temperature amplitudes again lead to negative NPP values during dry months and higher plant productivities with increasing by southern latitudes.

The transect shown here can be compared with the one given by Heimann et al. (1989, their Fig. 2) which is a result of a diagnostic, NDVI-based model (see 'Discussion' below).

4.2.2. Latitudinal-seasonal patterns

To obtain a global picture of the temporal development of the simulation results we reduced the spatial resolution of these flux values by summing up the carbon fluxes in latitudinal belts of 5° width. It should be noted, however, that each belt contains a different amount of area covered with vegetation. The belt's boundaries, the areas with vegetation cover and the number of grid elements can be seen from the first 3 columns of Table 4.

In Table 4 the numerical values of the latitudinal means of NPP are given for a latitudinal resolution of 5°. The values in column 2 show that the vegetation-covered area of the southern hemisphere is much smaller than that in the northern hemisphere; this fact is reflected in the absolute amplitude of NPP. In the last column of the table the sum of all monthly values of NPP (annual NPP in latitudinal belts of 5° width) is shown. The last row contains the sum of the values in the columns above. The 47999 grid elements, which were examined in this study cover an area of 106.2×10^6 km^2; the global annual NPP of the terrestrial biosphere amounts to 50.28 Gt C, given in the lower right corner of Table 4. Land deserts constituting an area of 21.6×10^6 km^2 with 8400 grid cells are not considered here.

As can be seen in Fig. 8 the seasonality of NPP is not very pronounced in the equatorial zones; however, the northern zones, especially the temperate and boreal forests, show strong variations in carbon fluxes over the year. Comparing seasonal values of NPP and heterotrophic respiration, the general patterns seem to be similar; however, the seasonal course of RES does not show amplitudes and gradients as strong as those of NPP.

In the climax steady-state calculation presented, the annual values of NPP and RES are equal to one another. By calculating the monthly difference between NPP and RES the net ecosystem productivity (NEP) is obtained, which is also displayed in Fig. 8. It can be seen that the whole ecosystem (terrestrial vegetation + soil) takes up carbon in the northern summer (June to September). During the rest of the year the vegetation in the northern zone acts as a weak source.

In the northern part of the tropics uptake fluxes appear during July to December and in the southern tropics during January to June. It is remarkable that the tropical region shows a seasonal course in NEP that is shifted by nearly 6 mo between north and south. However, the seasonality is not very pronounced in the tropics.

As the phenophases of the vegetation are explicitly simulated in the FBM, it is possible to compare the times of leaf shooting and abscission in regions with seasonal vegetation with data from phenological examinations (Lüdeke et al. 1994). Furthermore, the explicit simulation of the phenophases offers the possibility of comparing the simulation results with data from satellite observation (Lüdeke et al. 1996).

5. DISCUSSION

The FBM, as one representative of a group of ecosystem models, uses a unique mechanistic method of modeling that satisfies some optimality criteria. Therefore the results should not only be compared with the measured data, but also with the results of other models. At the present stage of development, the most interesting results are the seasonal course of NPP and LAI. Therefore the discussion will focus on them.

The annual global NPP of the FBM is prescribed by a vegetation map and the fixed mean annual NPP for each vegetation type (Fung et al. 1987). The resulting value of the annual NPP of 50.28 Gt C for the sum of all ecosystems indicates a reasonable choice of input parameters for the annual NPP.

In the first step we compare the values of the annual NPP, averaged over 30° latitude belts, obtained with the FBM to those obtained with the model CASA (Potter et al. 1993). Both the total value of NPP and the corresponding mean net primary productivities per unit area are shown in Table 5. Within CASA, the NPP values are derived from the intercepted photosynthetically active radiation (IPAR) and a light-use efficiency, ε, that is modified by temperature and soil moisture, while for the FBM, the area-averaged NPP values are derived from ecological estimates, which serve as input data for other detailed regional and seasonal results.

It can be concluded from the last row of Table 5 that both the total NPP and the mean values per unit area do not differ very much between the 2 models. However, the variation in mean productivities along the north-south gradient is much more pronounced in the CASA

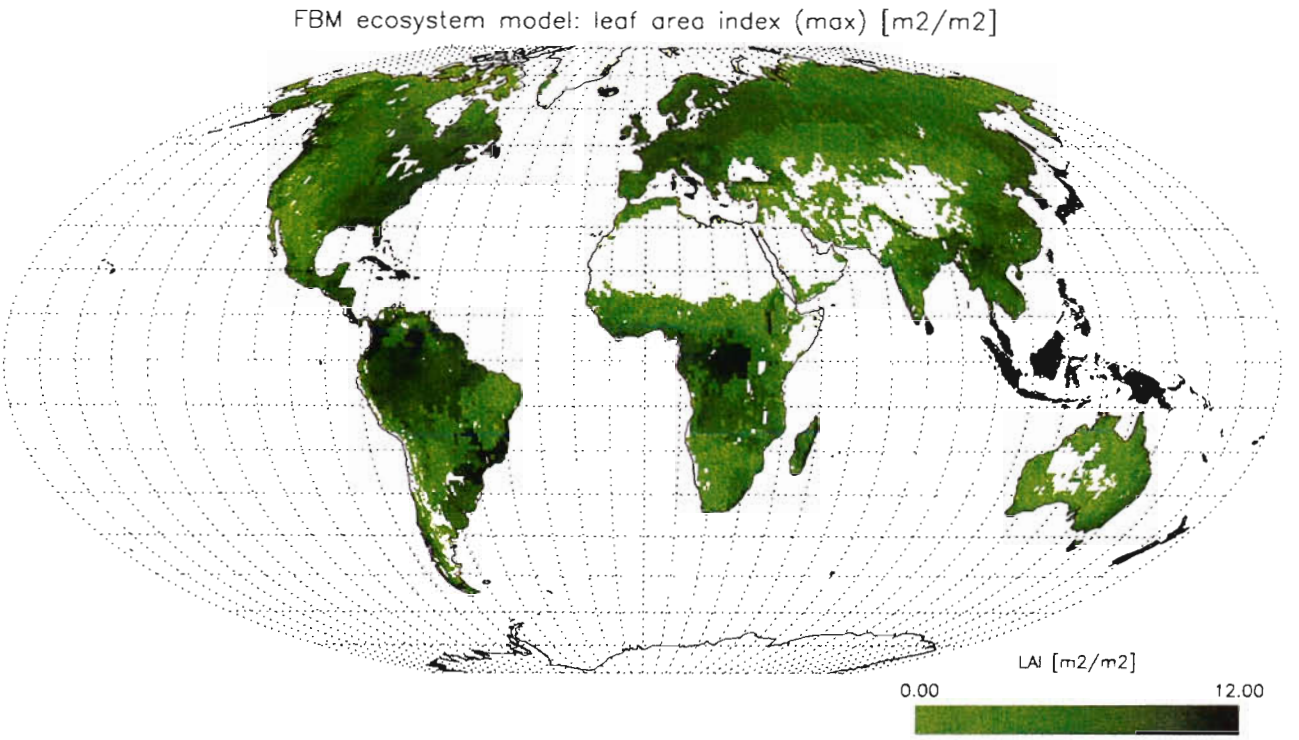

Fig. 6. Annual values of the global maximal leaf area index (LAI_{max}, $m^2\ m^{-2}$) as simulated by the FBM

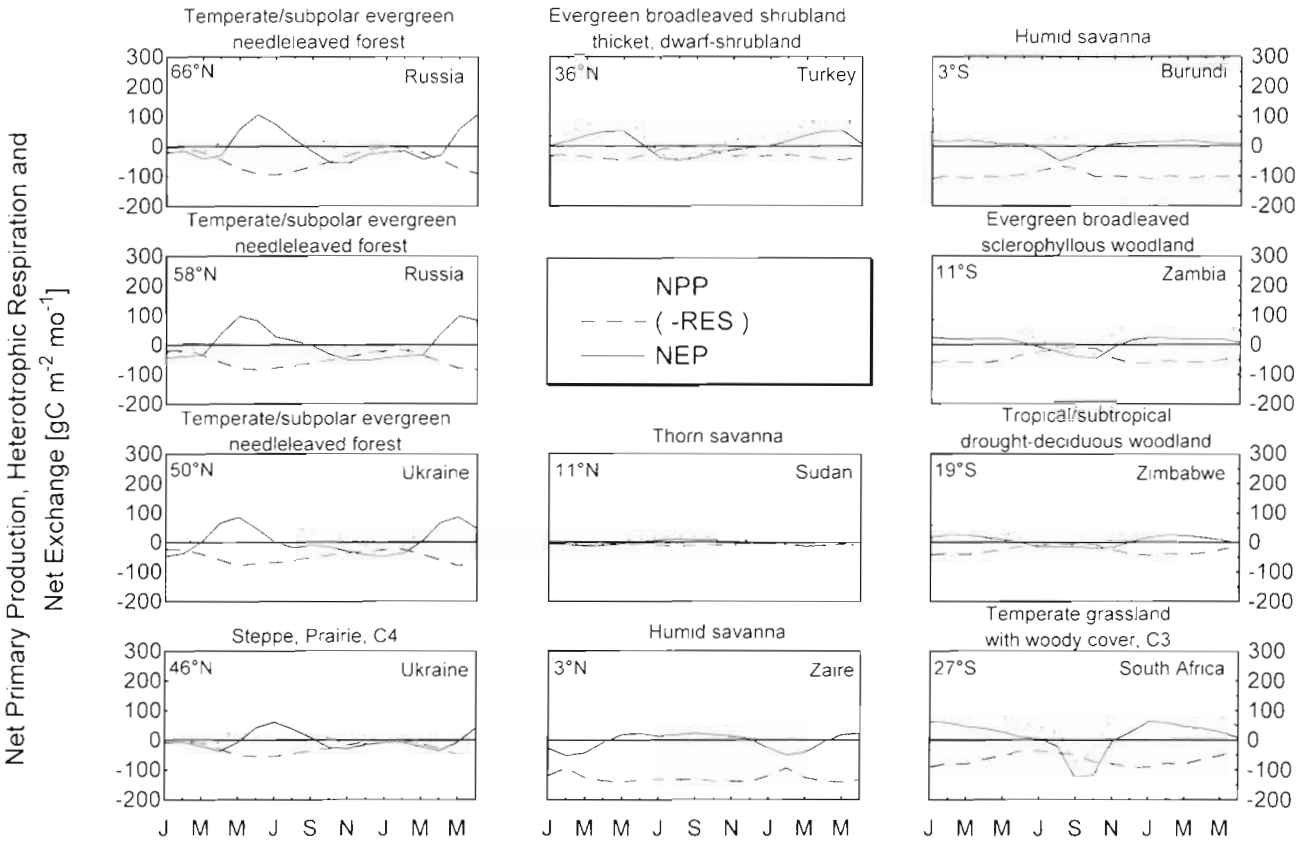

Fig. 7. Seasonal cycle of net primary productivity (NPP), negative of the heterotrophic respiration (−RES), and net ecosystem productivity (NEP) along a transect at 30° E extending from northwest Russia to South Africa. Each curve represents the flux over land for a grid square of 0.5° The first 6 mo of each cycle are displayed twice to reveal the cycle's annual variation more clearly. We plotted the negative of heterotrophic respiration to ease comparison with Heimann et al. (1989, their Fig. 2)

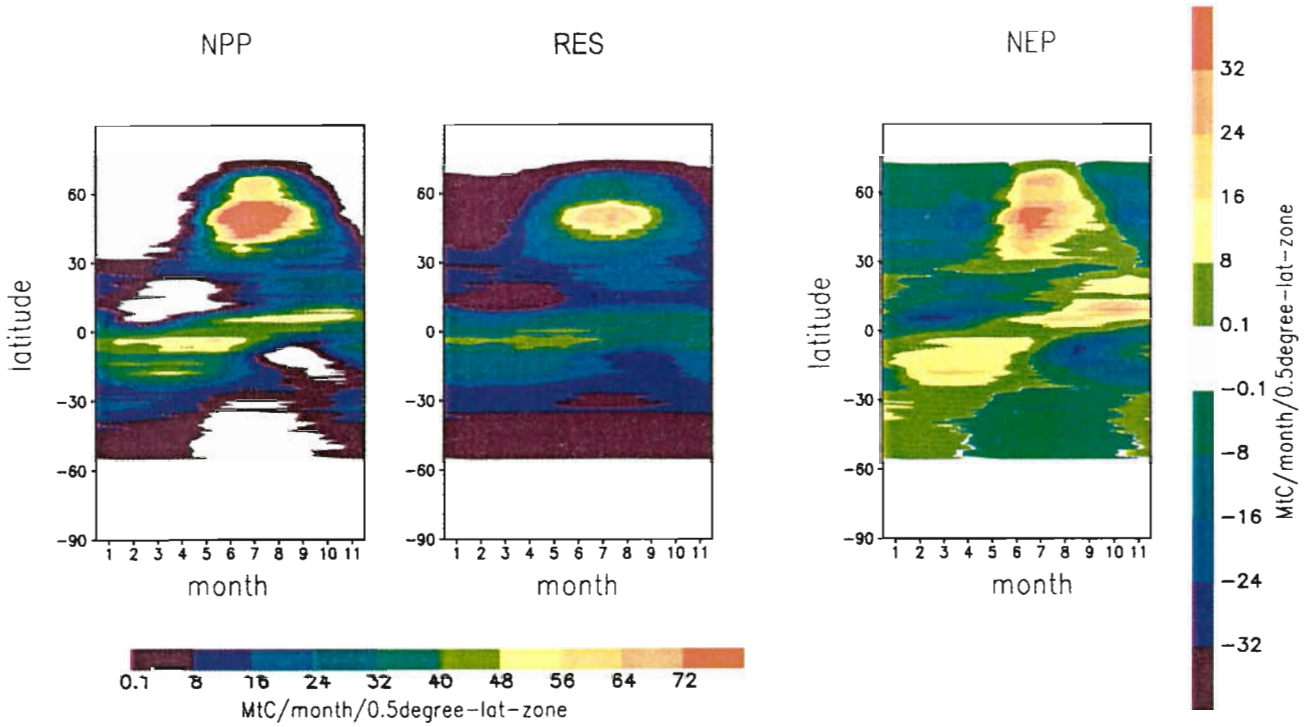

Fig. 8. Latitudinal means of monthly values of net primary productivity (NPP, Mt C mo^{-1}), heterotrophic respiration (RES, Mt C mo^{-1}), and net ecosystem production (NEP = NPP – RES, Mt C mo^{-1}) versus time

model (the productivities differ by a factor of 6) than in the FBM (the productivities differ by a factor of 3).

Within the FBM the individual climate of a grid element is taken into consideration to calculate the NPP, with the boundary condition that the prescribed average NPP value of a particular vegetation type is maintained. Comparison of the annual NPP of one grid element—which can be remarkably different from mean annual NPP for a given vegetation type—with well-established measured data [TEM (Raich et al. 1991) and MIAMI (Lieth 1975) calibration sites] provides another means of validation.

Fig. 9 shows such a comparison, with a fairly good agreement of measured and calculated data. In such comparisons, the scaling problem needs to be considered (measurements for several m^2 vs simulation data for areas up to 2500 km^2). Due to local site differences, there may be considerable variation within the area of any one modelled grid element, such that it is not surprising to find deviations from the 45 degree line.

The mechanistic modelling and prediction of the seasonal course of NPP is a special property of the FBM and therefore it is an interesting result for comparison. In Fig. 10 the monthly NPP values of the FBM and the TEM are compared for 5 selected locations. Both models used the CLIMATE database version 2.1 (Cramer, Potsdam, pers. comm.) for precipitation with the monthly values characteristic for each location, as given in the 5 diagrams. The scale for temperature (°C), and for precipitation (cm mo^{-1}) was chosen so that a single scale could be used for both of these climate parameters.

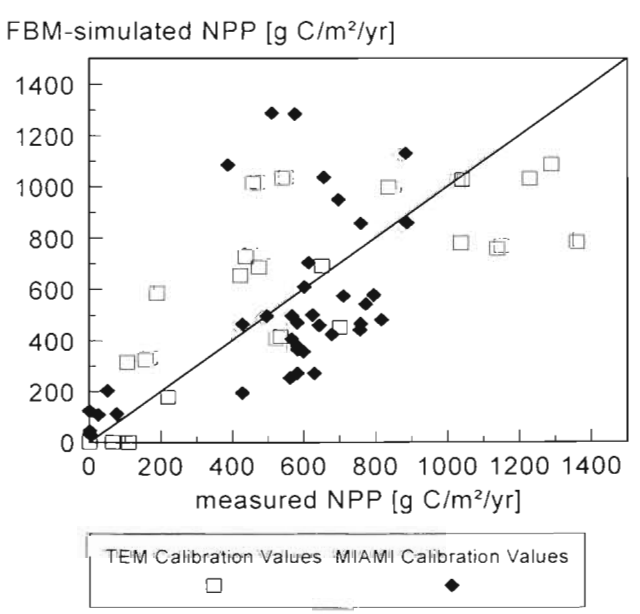

Fig. 9. Comparison of measured and simulated NPP values for grid elements of the TEM and MIAMI calibration sites

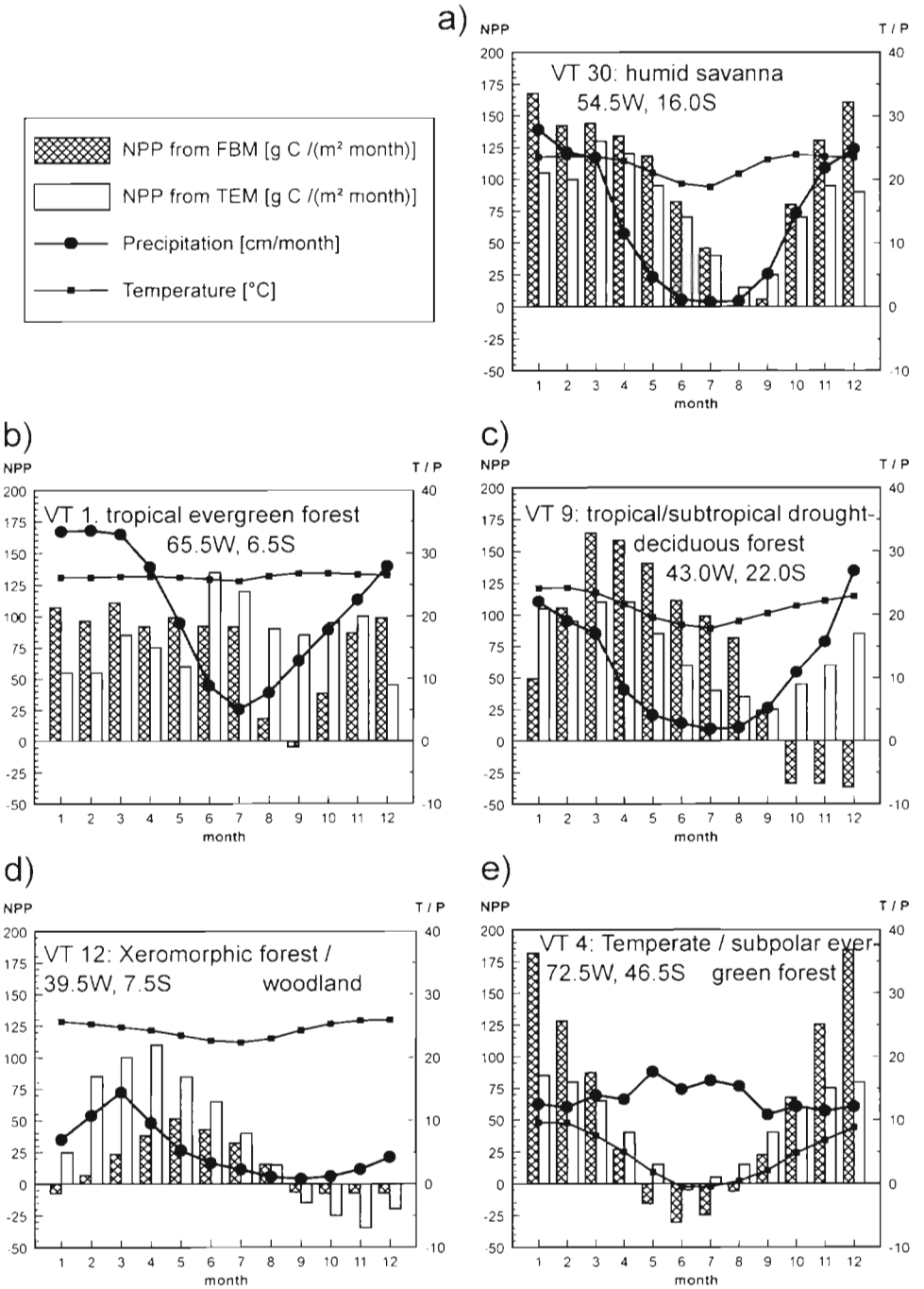

Fig. 10. Comparison of the monthly values of NPP simulated by the FBM and the TEM at 5 selected locations in South America. Within the figure 10°C corresponds to 10 cm precipitation per month, which is different from the climate diagrams of Walter, where 10°C is chosen to correspond to 20 mm precipitation (the corresponding Walter diagrams can be obtained by scaling down e.g. the mean monthly temperatures by a factor of 5)

It can be seen that the mean annual NPP values do not differ very much between models for locations (a) to (c), while in location (d) the mean annual value of NPP is higher in TEM, with the opposite result occurring in location (e). In location (a) there is a good correspondence between the 2 models with respect to seasonality; the minimum of production occurs 1 to 2 mo after the minimum in precipitation, resulting from the delayed soil water deficit. The same is true for location (e); however, in this case the minimum in productivity is due to the low temperature. In location (b) the productivity as derived in the FBM is influenced by the

Table 5. Comparison of latitudinally averaged productivity values simulated with the models CASA and FBM

Belt (° lat.)	NPP, CASA (Gt C yr^{-1})	Mean NPP, CASA (g C yr^{-1} m^{-2})	NPP, FBM (Gt C yr^{-1})	Mean NPP, FBM (g C yr^{-1} m^{-2})	Vegetation-covered area in FBM (10^3 km^2)
90.0 to 60.0	1.75	126.9	2.94	213.3	13785
60.0 to 30.0	10.28	263.3	15.61	399.8	39048
30.0 to 0.0	13.97	626.1	13.52	606.0	22312
0.0 to -30.0	20.04	757.9	16.04	606.7	26440
-30.0 to -60.0	1.95	422.6	2.18	472.5	4614
Total	48.02	452.2	50.28	473.5	106199

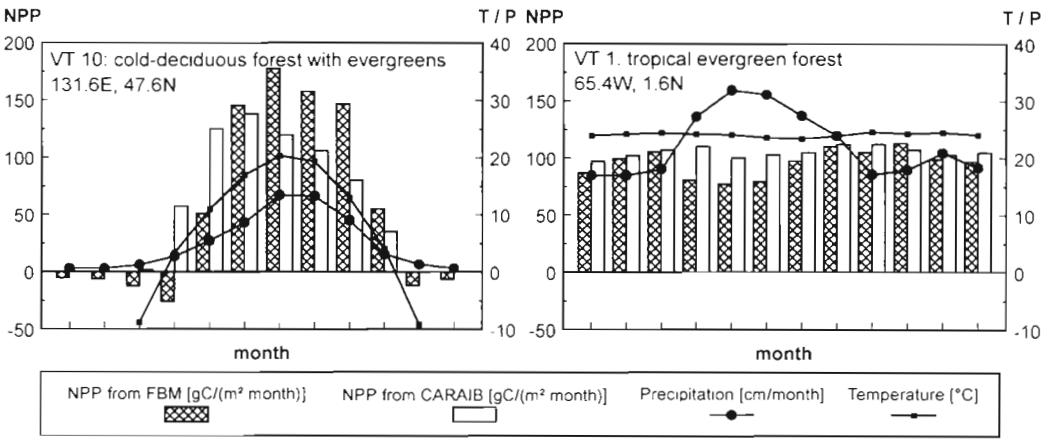

Fig. 11. Comparison of the monthly values of NPP simulated by the FBM and the CARAIB at 2 selected locations in the temperate and tropical zone. Within the figure 10°C corresponds to 10 cm precipitation per month, which is different from the climate diagrams of Walter, where 10°C is chosen to correspond to 20 mm precipitation

precipitation minimum, whereas such an effect cannot be seen in the predicted values of TEM. In scaling down the temperature curve at site (b) by a factor of 5 to obtain the Walter diagram characteristics of drought conditions, the temperature and precipitation curves just become tangents of each other in July, thus indicating the beginning of a water deficit. Evidently, the FBM is somewhat more sensitive to water stress than the TEM. We notice for site (c) a strong seasonal behaviour for both models; again the minimum is delayed by several months relative to the precipitation minimum. For site (d) we notice a higher productivity in TEM; both models show negative NPP values in the last 4 months of the year. In summary we conclude that there is a good correlation between the seasonal productivities calculated in the 2 models, with a stronger sensitivity to water stress in the Frankfurt model.

The comparison of the FBM results with those of the CARAIB (Warnant et al. 1994), depicted in Fig. 11, underlines the impression that both models agree within a broad context.

Certainly the annual NPP values are in very good agreement (CARAIB is restricted to non-negative monthly NPP values). For the broad-leaved seasonal forest one recognizes that the maximum monthly production of the FBM occurs at a later point in time relative to the CARAIB. The comparison for the equatorial rainforest underlines the somewhat more pronounced seasonality in the FBM.

Lüdeke et al. (1996) compared the leaf shooting day for cold-deciduous and mixed forests predicted by the FBM with the corresponding leaf emergence derived from NDVI data (Fig. 12). The abscissa shows the position of the leaf shooting day for the particular grid elements relative to the NDVI-derived time interval $[t_1, t_2] = [0, 1]$ which corresponds to the time period where the NDVI signal rises (single-line-hatched area). Within the figure the cross-hatched area corresponds to the leaf shooting days derived from phenological gardens for this particular vegetation type.

One can conclude that the centers of all 3 estimates overlap strongly while a detailed consideration shows

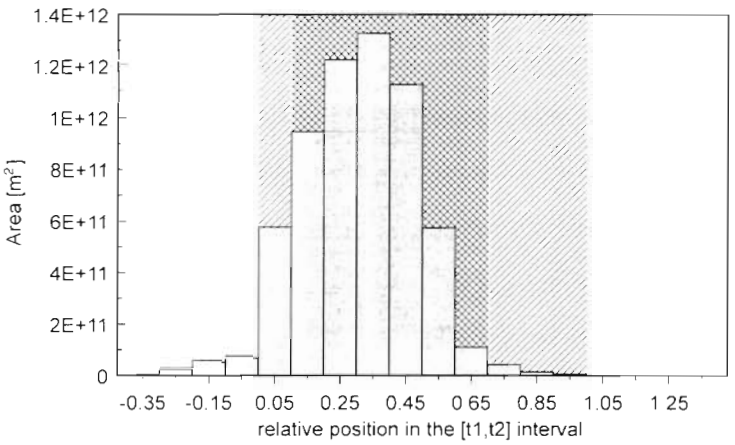

Fig. 12. Frequency distribution of the relative position of the FBM-predicted shooting dates for cold-deciduous and mixed forests (3280 grid elements of 5° × 5°, referring to actual vegetation, were considered) in the $[t_1, t_2]$ interval = [0,1] which corresponds to the time period when the NDVI signal rises (single-line-hatched area). The cross-hatched area shows the time period when leaf shooting days were observed in phenological gardens for these particular vegetation types

that the FBM-predicted leaf emergence dates are somewhat earlier than observed in the phenological gardens. There the leaf emergence refers to the trees, which are dominant in this vegetation type, while the understory is excluded. In the NDVI-derived time span, the satellite observations include the understory, so it is not surprising that the initial phase of increasing NDVI is somewhat earlier than the onset of leaf shooting derived from the phenological gardens. Within the FBM, forest and woody vegetation types again refer to the phenology of trees, which explains the very good correlation between the center of the leaf emergence date predicted by the FBM and that observed within the phenological gardens (Schnelle 1985). Again, the FBM leaf shooting days occur later than the NDVI-derived results for the composite of under- and overstory.

To summarize, one can state that, relative to the 2 models TEM and CARAIB, the FBM shows a characteristic leaf shooting day which is later in the year, whereas relative to the data derived from the phenological gardens its predicted dates of leaf emergence are rather early. It is therefore believed that the FBM results are in good agreement with the observations.

6. CONCLUSIONS AND PROSPECTS FOR FURTHER DEVELOPMENT

With the global process-oriented Frankfurt Biosphere Model we have focused in this paper on the seasonal and regional CO_2 exchange between 32 vegetation types and the atmosphere. The experiments were performed with the steady-state reference climate of the CLIMATE database version 2.1 (Cramer, Potsdam, pers. comm.) for potential vegetation in its corresponding equilibrium state. The allocation scheme presented, in which assimilated carbon flows to the green biomass and remaining biomass (**GC** and **RC**) over the seasons of the year, allows us *ab initio* to calculate the leaf emergence dates, the seasonal course of the leaf area index (LAI) and the maximal LAI, which are in good agreement with the observations for phenological gardens and with evaluations of the seasonal behaviour of the NDVI (Lüdeke et al. 1996). In a selected transect at 30° E the model predicts the performance of the ecosystems as expected from ground truth. In an intercomparison with other biosphere models (Lurin et al. 1994) having a similar structure there is good agreement in the seasonal and regional behaviour of NPP fluxes and heterotrophic respiration fluxes. The resulting CO_2 source-sink pattern as shown in Fig. 8 has been validated within the Stanford EPRI Research Project CCMLP (carbon cycle model linkage project) by coupling it to the Hamburg atmospheric transport model (together with fossil fuel emissions and oceanic sources and sinks) and comparing the simulated atmospheric CO_2 signal with the observed seasonal cycle at 27 monitoring stations. The average mean squared error for all stations was lowest for the FBM as compared to the other 5 prognostic models included in this study (M. Heimann et al. unpubl.).

Several other experiments with the FBM using non-equilibrium calculations have been performed and are of particular interest with respect to future climate changes. As a first test the well-studied period between 1980 and 1993 was evaluated: the response of the FBM to temperature and precipitation anomalies correlated well with the observed interannual signal of atmospheric CO_2 (Kindermann et al. 1996).

The FBM has been conceived from its beginning as a transient biosphere model with the ability to predict the performance of an ecosystem from the plant seedling to its climax state. In particular, the forests of the temperate zone (boreal needle-leaved, cold-deciduous and mixed forests) have been examined in the transient mode for the present climate, a future $2 \times CO_2$ climate and a combination of climate change coupled to a corresponding CO_2 increase (Häger et al. 1996).

The 2 latter studies use a more realistic model for dead organic matter (Nadler 1994) with 2 litter compartments (rapidly and slowly decomposing) and 1 humus compartment (very slowly decomposing).

Appendix 1

A1. Model equations

Carbon assimilation:

The effective carbon assimilation rate, C_{ASS}, can be considered as a function of the product of a term dependent on light and canopy structure, a temperature-dependent term and a soilwater-dependent term. The dependence on irradiance and leaf area index, LAI, which is associated with the **GC** compartment is modelled taking into account the light attenuation in the canopy. For the temperature dependence an optimum curve is used characterized by the minimum, maximum, and optimum temperature of photosynthesis. The dependence of photosynthesis on water availability, represented by the soil water content **SW**, is assumed to follow a saturation curve which is 0 at the permanent wilting point and approaches 1 for field capacity.

$$C_{ASS} = \alpha \cdot \mathrm{LAI}(\mathbf{GC}) \cdot h_1[I, \mathrm{LAI}(\mathbf{GC})] \cdot h_2(T) \cdot h_3(\mathbf{SW}) \quad \text{(A1)}$$

Light-dependent factor h_1:

$$h_1 = \frac{1}{k \cdot \mathrm{LAI}} \cdot \ln\left(\frac{\frac{\alpha}{\Phi} + I}{\frac{\alpha}{\Phi} + I \cdot e^{(-k\,\mathrm{LAI})}} \right) \quad \text{(A2)}$$

where α is the photosynthetic capacity per unit leaf area, Φ is the initial quantum yield, I the light intensity of PAR and k the extinction coefficient of the canopy.

Temperature-dependent factor h_2:

$$h_2(T) = \frac{2}{\alpha \cdot \mathrm{SLA}} \cdot \left\{ a_T \cdot \frac{(T - T_{min}) \cdot (T - T_{max})}{(T - T_{min})(T - T_{max}) - (T - T_{opt})^2} + \beta \cdot e^{\omega(T - T_0)} \right\} \quad \text{(A3)}$$

where SLA is the specific leaf area, T_{min}, T_{opt} and T_{max} are the cardinal points of net photosynthesis and the term in brackets reflects the contribution of autotrophic respiration with a_T being a normalization factor for h_2 and T_0 being the reference temperature for autotrophic respiration (T_0 = 293 K).

Moisture-dependent factor h_3:

$$h_3(\mathbf{SW}) = \frac{\tanh\left(a_{SW} \frac{\mathbf{SW} - \mathrm{PWP}}{\mathrm{AWC}} \right)}{\tanh(a_{SW})} \quad \text{(A4)}$$

where a_{SW} is an adjustment parameter such that, for a relative moisture content of 50 %, $h_3(\mathbf{SW})$ = 0.75 as proposed by Larcher (1984); and PWP, FC and AWC refer to the permanent wilting point, field capacity and available water capacity, respectively.

***Autotrophic respiration for* GC:**

Autotrophic respiration C_{GA} and C_{RA} for compartments **GC** and **RC** respectively, is modelled similarily for both compartments, depending on the compartment size and an exponential function of the temperature corresponding to a constant Q_{10} value for each ecosystem type, exposed here by the parameter ω listed in Table A2; α, β, γ, δ, and ε are calibration parameters as listed in Table A4.

$$C_{GA} = \beta \cdot \mathbf{GC} \cdot e^{\omega(T - T_0)} \quad \text{(A5)}$$

***Autotrophic respiration for* RC:**

$$C_{RA} = \gamma \cdot \mathbf{RC} \cdot e^{\omega(T - T_0)} \quad \text{(A6)}$$

***Litter production for* RC:**

The litter production C_{GS} and C_{RS} for the 2 compartments is assumed to be proportional to the respective compartment size.

$$C_{RS} = \delta \cdot \mathbf{RC} \quad \text{(A7)}$$

***Litter production for* GC:**

Litter production of the **GC** compartment for the evergreen vegetation types is given by:

$$C_{GS} = \varepsilon \cdot \mathbf{GC} \quad \text{(A8)}$$

For the **GC** compartment of the deciduous vegetation types an additional constant-rate litter production occurs during the abscission phase.

Litter production of the **GC** compartment for the leaf abscission phase of deciduous vegetation types is given by:

$$\bar{C}_{GS} = \frac{\Omega^{-1}(\mathbf{RC}) - \Theta^{-1}(\mathbf{RC})}{\tau_{III}} \quad \text{(A9)}$$

where τ_{III} refers to time of leaf abscission, taken to be 1 mo. For the dormancy phase, the total litter production is assumed to be proportional to the standing biomass **BC**:

$$\bar{C}_{BS} = \delta \cdot (\mathbf{GC} + \mathbf{RC}) \quad \text{(A10)}$$

Heterotrophic respiration:

To model the response of the decomposition of dead organic matter, C_{SA}, to climate, we extended the model of Fung et al. (1987) taking into consideration a linear dependence on compartment size and introducing a soil moisture factor analogous to the moisture dependence of photosynthesis. The temperature dependence of the organic matter decomposition is divided into 4 respiration groups (RG = 1, 2, 3, 4) which depend on the vegetation type. Temperate/boreal needle-leaved forests and woodlands (RG = 3) and temperate/boreal broad-leaved forests and woodlands (RG = 2) obey the same functional form:

$$C_{SA} = \begin{cases} \eta \cdot h_3(\mathbf{SW}) \cdot (1 + q_{RG} \cdot T) \cdot \mathbf{SC} & \text{for } q_{RG} \cdot T > -1 \\ 0 & \text{otherwise} \end{cases} \quad \text{(A11)}$$

where q_{RG3} = 0.07 and q_{RG2} = 0.16. Tropical/subtropical woody vegetation (RG = 1) and all grasslands (RG = 4) are parameterized to follow the function:

$$C_{SA} = \begin{cases} \eta \cdot h_3(\mathbf{SW}) \cdot \left(1 + q_{RG} \cdot \frac{T}{T_{max}}\right) \cdot \mathbf{SC} & \text{for } q_{RG} \cdot T > -1 \\ 0 & \text{otherwise} \end{cases} \quad \text{(A12)}$$

where q_{RG1} = 5.57 and q_{RG4} = 25.67. T and T_{max} in these equations are expressed in °C, and T_{max} refers to maximum monthly air temperature.

Water fluxes:

Due to the close relation between assimilation and transpiration, the actual evapotranspiration, W_{SA}, is calculated as the product of potential evapotranspiration as in Thornthwaite (1948), W_{PET}, and the soilwater-dependent function as used in the calculation of assimilation.

Appendix 1 (continued)

W_{Runoff} comprises both surface runoff and drainage. It is taken as the surplus water when the soil water content reaches field capacity.

$$W_{SA} = W_{PET} \cdot h_3(\mathbf{SW}) \quad (A13)$$

A2. Global radiation

Global radiation, S (W m^{-2}), the direct and diffuse shortwave radiation impinging on the canopy, is a function of the radiation S_0 at the outer edge of the atmosphere, the elevation angle of the sun, β, and the cloud cover. In the CLIMATE database version 2.1 (Cramer, Potsdam, pers. comm.) cloud cover is expressed as the ratio of actual hours of bright sunshine, n, to the maximum possible sunshine hours, N. Therefore we use the Ångström relationship in the following way (Swift et al. 1976, Jones 1992, Friend pers. comm.):

$$S = S_0(t_d) \cdot \sin\beta \cdot \left(0.251 + 0.509\frac{n}{N}\right) \quad (A14)$$

Due to the seasonal variations in the distance between the sun and the earth, the radiation at the outer edge of the atmosphere, the 'solar constant' S_0, is not a perfect constant but varies slightly (±3%) during the year:

$$S_0(t_d) = \frac{1368}{\left\{1 - 0.016729\cos\left[0.9856(t_d - 4) \cdot \pi/180\right]\right\}^2} \quad (A15)$$

The sun elevation angle is calculated as a function of the day t_d ($1 \le t_d \le 365$) and the hour t_h ($1 \le t_h \le 24$):

$$\sin\beta = \sin\lambda \sin\delta + \cos\lambda \cos\delta \cos h \quad (A16)$$

$$\delta = -23.4856\frac{\pi}{180} \cdot \cos\left(\frac{2\pi(t_d + 10)}{365.25}\right) \quad (A17)$$

$$h = \frac{2\pi}{24} \cdot (t_h - 12) \quad (A18)$$

where
S = shortwave radiation at the top of the canopy (W m^{-2})
S_0 = shortwave radiation at the outside of the atmosphere (W m^{-2})
n = actual hours of bright sunshine (h)
N = maximum possible sunshine hours (h)
t_d = number of the day in the year (d)
t_h = hour of the day (h)
λ = geographical latitude (rad)
δ = solar declination (rad)
β = sun elevation angle (rad)
h = hour angle of the sun (rad)
Photosynthetically active radiation, PAR, is assumed to be 50% of the global radiation S and can be identified with the variable I in Eqs. (A1) & (A2).

A3. Classification of soil hydrological properties

In order to determine relative volumetric water content Θ_{soil} at PWP and FC for each soil texture class we use the parameterisation of the composition dependence of the soil water potential given by Saxton et al. (1986). He derived the parameters A and B for the characteristic equation which relates the soil water potential ψ_{soil} to Θ:

$$\psi_{soil} = A \cdot \Theta_{soil}^{B} \quad (A19)$$

where A and B are functions of the soil texture composition and therefore can be determined for each soil texture class by applying:

$$A = 100\exp\left(-4.396 - 0.0715(\%C) - 4.88 \cdot 10^{-4}(\%S)^2 - 4.285 \cdot 10^{-5}(\%S)^2(\%C)\right) \quad (A20)$$

$$B = -3.140 - 0.00222(\%C)^2 - 3.484 \cdot 10^{-5}(\%S)^2(\%C) \quad (A21)$$

For field capacity we use a soil water potential of −15 kPa (Larcher 1984) whereas for the permanent wilting point −1.5 MPa was chosen, except for the desert plants and xerophytes, where we chose a value of −3.5 MPa.

Table A1 (following this Appendix) lists the relative fractions of clay (%C) and sand (%S), taken from the texture triangle as given by the FAO/UNESCO (1974-1981) for each of the Zobler soil texture classes.

A4. Classification of vegetation types

Table A2 contains the ecophysiological and miscellaneous model parameters of the 32 vegetation types examined. The RG group describes the temperature dependence of organic matter decomposition, SLA is the specific leaf area index, T_{min}, T_{max}, and T_{opt} describe the cardinal points of photosynthesis as derived from Larcher (1984), ω as shown in Table A2 refers to the temperature dependence of autotrophic respiration, and ξ, κ, and ν are parameters of the allometric relationships described in Eqs. (2) & (3).

Table A3 describes parameters derived from ecological estimates. $\mathbf{GC}_{max}$, $\mathbf{RC}_{max}$, and $\mathbf{SC}_{max}$ refer to the maximum carbon mass of the corresponding compartments; the fluxes NPP (net primary production), ResG (autotrophic respiration of the **GC** compartment) and LpG (litter production of the **GC** compartment) refer to the corresponding climax state. From Eqs. (7) to (10) along with the relation derived in Section A5 of this Appendix, the following equalities are assumed:

$$\text{ResG} = \text{ResR}$$
$$\text{LpG} = a_1\,\text{LpR}$$

where a_1 = 1 for 29 vegetation types, except for type 30 where a_1 = 2 and for type 36 and 37 where a_1 = 10/9; and

$$\text{GPP} = \text{NPP} + 2\text{ResG}$$

Table A4 is strictly concerned with the model parameters α, β, γ, δ, ε, and η derived in the calibration procedure, described in detail in Lüdeke et al. (1994).

A5. Derivation of LpG/LpR ratio

In the FBM we chose a ratio of 1/1 to represent the ratio of litter production from the green and remaining carbon masses, LpG/LpR, for all forests, woodlands and shrublands

Appendix 1 (continued)

and most of the grasslands. At first, this may seem surprising, especially for forest ecosystems. According to Rodin & Bazilevich (1968) and Bray & Gorham (1964) the annual aboveground litter production from **GC** and **RC** has a ratio of 7/3. However, for total litter production we need to include:

(1) the belowground litter production, here expressed by the ratio of aboveground to belowground litter production from **GC** and **RC** (ρ_G, ρ_R); and
(2) the rate of additional litter production from falling trees, LpT = $\mathbf{RC}_{max}$/lifetime, not included in the field experiments measuring LpR'
With NPP = LpG + LpR' + LpT we derived:

$$\frac{LpG}{LpR} = \frac{NPP - LpT}{NPP \cdot \frac{3\rho_G \cdot (\rho_R + 1)}{7\rho_R \cdot (\rho_G + 1)} + LpT} \qquad (A22)$$

Choosing $\rho_G = 1$ is analogous to the partitioning of **GC** into leaves and feeder roots. Assuming, in accordance with experiments, $\rho_R = 2$ and a mean lifetime of woody plants of 100 yr the above formula yields for the (NPP, $\mathbf{RC}_{max}$) sets (see Table A3) a LpG/LpR ratio of approximately 1.

This result is not very sensitive concerning variation of ρ_G and ρ_R (a 1% change of ρ_G leads to only a 0.2% change of LpG/LpR), whereas a relative change in LpT yields a change in LpG/LpR of equal magnitude. The value of LpT depends on the difficult estimation of the mean lifetime of woody plants. In light of these uncertainties we fixed LpG/LpR at 1 for all woody vegetation types.

In the case of evergreen vegetation types this ratio (for given values of NPP and $\mathbf{GC}_{max}$) results in a mean lifetime for needles of $\tau_N = 2\mathbf{GC}_{max}$/NPP. This lifetime lies within the expected range of all evergreen vegetation types and thus underlines the consistency of our ecological estimations.

Table A1. Assignment of relative compositions from the FAO texture triangle to the soil texture classes considered

	Zobler soil texture:						
	Coarse	Coarse + medium	Medium	Coarse + fine	Coarse + medium + fine	Fine	Medium + fine
% Sand	83	60	37	50	46	17	27
% Silt	8	20	33	12	19	17	25
% Clay	9	20	30	38	35	66	48

Table A2. Ecophysiological and miscellaneous model parameters

VT	Code	RG	SLA (m^2 kg^{-1} C)	T_{min} (K)	T_{max} (K)	T_{opt} (K)	ω (K^{-1})	ξ [(kg C m^{-2})$^{1/\kappa}$]	κ	ν [(kg C m^{-2})$^{1/\kappa}$]
1.	FHMBE	1	20.0	275.6	320.6	300.6	0.0642	27.23	1.6	–
2.	FHSBE	1	17.0	275.6	320.6	300.6	0.0642	21.81	1.6	–
3.	FHIBE	1	17.0	275.6	320.6	300.6	0.0642	21.81	1.6	–
4.	FTMBE	2	30.0	270.1	316.6	298.1	0.0642	41.84	1.6	–
5.	FTSBE	2	30.0	271.1	315.6	293.1	0.0642	41.84	1.6	–
6.	FTSXE	2	23.0	270.1	316.6	298.1	0.0642	36.02	1.6	–
7	FHSNE	3	12.0	275.6	320.6	300.6	0.0642	9.00	1.6	–
8.	FCDNE	3	12.0	270.6	311.6	290.6	0.0642	5.49	1.6	–
9.	FHSBD	1	40.0	275.6	320.6	300.6	0.0642	46.47	1.6	828.91
10.	FTMAC	2	40.0	273.0	313.0	294.0	0.0642	96.38	1.6	1694.42
11	FCSAC	2	40.0	273.0	313.0	294.0	0.0642	96.38	1.6	1694.42
12.	WHSXD	2	23.0	270.1	316.6	298.1	0.0642	22.03	1.6	109.67
13.	WHSBE	2	16.0	270.1	316.6	298.6	0.0642	23.61	1.6	–
14.	WCDNE	3	12.0	270.6	311.6	290.6	0.0642	5.01	1.6	–
15.	WHSBD	1	27.0	275.6	320.6	300.6	0.0642	21.23	1.6	50.29
16.	WCDNC	3	27.0	273.0	313.0	294.0	0.0642	30.81	1.6	112.76
20.	STDBE	2	12.0	271.6	316.6	298.1	0.0642	27.96	1.6	–
21.	SCDNE	3	12.0	270.6	311.6	290.6	0.0642	47.67	1.6	–
22.	STDBD	2	20.0	271.6	316.6	298.1	0.0642	8.76	1.6	16.01
23.	SCDBC	4	20.0	270.1	313.1	288.1	0.0336	10.91	1.6	22.31
24.	SHSXE	2	20.0	275.6	320.6	300.6	0.0642	45.35	1.6	–

Table A2 (continued)

VT	Code	RG	SLA (m^2 kg^{-1} C)	T_{min} (K)	T_{max} (K)	T_{opt} (K)	ω (K^{-1})	ξ [(kg C m^{-2})$^{1/\kappa}$]	κ	ν [(kg C m^{-2})$^{1/\kappa}$]
25.	STDXD	2	20.0	271.6	316.6	298.1	0.0642	18.21	1.6	167.30
26.	SHDXE	2	20.0	275.6	320.6	300.6	0.0642	76.11	1.6	–
27	SCDTC	2	40.0	270.1	313.1	288.1	0.0336	7.28	1.6	13.93
30.	GHM4E	4	20.0	279.2	328.2	313.2	0.0531	12.72	1.2	–
31	GHS4D	4	20.0	279.2	328.2	313.2	0.0531	4.75	1.2	32.77
32.	GHD4E	4	20.0	279.2	328.2	313.2	0.0531	12.68	1.2	–
33.	GHD4D	4	40.0	279.2	328.2	313.2	0.0642	6.34	1.2	33.46
34.	GTM3D	4	20.0	272.2	318.2	298.2	0.0531	12.13	1.2	36.42
35.	GTM4D	4	20.0	279.2	328.2	313.2	0.0531	12.13	1.2	36.42
36.	GTD3D	4	22.0	272.2	318.2	298.2	0.0531	2.99	1.2	10.30
37	GTD4D	4	22.0	279.2	328.2	313.2	0.0531	2.99	1.2	10.30

Table A3. Ecological estimates of equilibrium carbon pool and annual flux sizes

VT	Code	GC_{max} (kg C m^{-2})	RC_{max} (kg C m^{-2})	SC_{max} (kg C m^{-2})	NPP (kg C m^{-2} yr^{-1})	ResG (kg C m^{-2} yr^{-1})	LpG (kg C m^{-2} yr^{-1})
1.	FHMBE	0.810	19.440	11.000	0.945	1.580	0.472
2.	FHSBE	0.790	14.960	10.000	0.800	1.080	0.400
3.	FHIBE	0.790	14.960	10.000	0.800	1.080	0.400
4.	FTMBE	0.396	9.504	14.000	0.760	0.710	0.380
5.	FTSBE	0.396	9.504	14.000	0.760	0.710	0.380
6.	FTSXE	0.340	6.410	12.000	0.300	0.225	0.150
7.	FHSNE	1.215	12.285	11.000	0.630	0.355	0.315
8.	FCDNE	1.026	5.724	14.000	0.310	0.155	0.155
9.	FHSBD	0.333	8.000	10.000	0.555	0.280	0.278
10.	FTMAC	0.324	15.880	12.000	0.540	0.270	0.270
11.	FCSAC	0.324	15.880	12.000	0.540	0.270	0.270
12.	WHSXD	0.225	2.025	4.000	0.285	0.140	0.142
13.	WHSBE	0.380	5.020	8.000	0.360	0.180	0.180
14.	WCDNE	1.080	5.670	9.000	0.350	0.180	0.175
15.	WHSBD	0.360	4.140	6.500	0.300	0.150	0.150
16.	WCDNC	0.324	5.076	8.000	0.360	0.180	0.180
20.	STDBE	0.220	2.480	7.000	0.290	0.150	0.145
21	SCDNE	0.160	2.540	10.000	0.200	0.100	0.100
22.	STDBD	0.430	2.270	4.500	0.270	0.135	0.135
23.	SCDBC	0.380	2.320	6.500	0.275	0.140	0.137
24.	SHSXE	0.048	0.352	2.000	0.060	0.030	0.030
25.	STDXD	0.080	0.320	2.000	0.120	0.060	0.060
26.	SHDXE	0.018	0.123	2.000	0.040	0.020	0.020
27	SCDTC	0.150	0.350	19.000	0.100	0.120	0.050
30.	GHM4E	0.300	3.000	6.000	0.900	0.675	0.600
31	GHS4D	0.250	0.900	5.500	0.400	0.300	0.200
32.	GHD4E	0.100	0.800	4.000	0.100	0.080	0.050
33.	GHD4D	0.100	0.400	5.000	0.150	0.113	0.075
34.	GTM3D	0.300	2.860	6.000	0.370	0.278	0.180
35.	GTM4D	0.300	2.860	6.000	0.370	0.278	0.180
36.	GTD3D	0.280	0.650	12.000	0.380	0.285	0.180
37	GTD4D	0.280	0.650	12.000	0.380	0.285	0.180

Table A4. Model parameters derived from ecological estimates through calibration

VT	Code	α (kg C m^{-2} s^{-1})	β (s^{-1})	γ (s^{-1})	δ (s^{-1})	ε (s^{-1})	η (s^{-1})
1.	FHMBE	9.487×10^{-8}	4.681×10^{-8}	1.895×10^{-9}	7.733×10^{-10}	1.907×10^{-8}	4.735×10^{-10}
2.	FHSBE	8.200×10^{-8}	4.044×10^{-8}	2.100×10^{-9}	8.478×10^{-10}	1.648×10^{-8}	5.038×10^{-10}
3.	FHIBE	8.620×10^{-8}	5.079×10^{-8}	2.637×10^{-9}	8.509×10^{-10}	1.645×10^{-8}	5.468×10^{-10}
4.	FTMBE	1.176×10^{-7}	1.543×10^{-7}	5.534×10^{-9}	1.282×10^{-9}	3.624×10^{-8}	9.101×10^{-10}
5.	FTSBE	5.130×10^{-8}	7.825×10^{-8}	3.011×10^{-9}	1.273×10^{-9}	3.382×10^{-8}	5.410×10^{-10}
6.	FTSXE	2.916×10^{-8}	3.199×10^{-8}	1.607×10^{-9}	7.482×10^{-10}	1.524×10^{-8}	3.336×10^{-10}
7.	FHSNE	3.404×10^{-8}	1.365×10^{-8}	1.333×10^{-9}	8.174×10^{-10}	8.423×10^{-9}	1.015×10^{-9}
8.	FCDNE	1.903×10^{-8}	1.422×10^{-8}	2.473×10^{-9}	7.004×10^{-10}	5.959×10^{-9}	8.170×10^{-10}
9.	FHSBD	4.985×10^{-8}	4.334×10^{-8}	8.616×10^{-10}	1.116×10^{-9}	–	4.183×10^{-10}
10.	FTMAC	5.659×10^{-8}	9.030×10^{-8}	1.071×10^{-9}	5.424×10^{-10}	–	7.904×10^{-10}
11.	FCSAC	7.087×10^{-8}	1.196×10^{-7}	1.383×10^{-9}	5.427×10^{-10}	–	1.034×10^{-9}
12.	WHSXD	4.348×10^{-8}	1.477×10^{-8}	1.817×10^{-9}	2.297×10^{-9}	–	7.755×10^{-10}
13.	WHSBE	3.320×10^{-8}	1.564×10^{-8}	1.145×10^{-9}	1.146×10^{-9}	1.559×10^{-8}	5.240×10^{-10}
14.	WCDNE	2.830×10^{-8}	1.773×10^{-8}	3.321×10^{-9}	9.905×10^{-10}	5.366×10^{-9}	1.655×10^{-9}
15.	WHSBD	1.900×10^{-8}	1.806×10^{-8}	9.605×10^{-10}	1.152×10^{-9}	–	3.374×10^{-10}
16.	WCDNC	8.932×10^{-8}	1.308×10^{-7}	5.129×10^{-9}	1.128×10^{-9}	–	3.019×10^{-9}
20.	STDBE	8.614×10^{-8}	2.757×10^{-8}	2.294×10^{-9}	1.899×10^{-9}	2.348×10^{-8}	6.073×10^{-10}
21.	SCDNE	1.492×10^{-7}	9.521×10^{-8}	5.184×10^{-9}	1.269×10^{-9}	2.503×10^{-8}	1.055×10^{-9}
22.	STDBD	3.781×10^{-8}	1.876×10^{-8}	2.385×10^{-9}	1.896×10^{-9}	–	9.251×10^{-10}
23.	SCDBC	3.626×10^{-8}	4.896×10^{-8}	4.388×10^{-9}	1.855×10^{-9}	–	2.602×10^{-10}
24.	SHSXE	3.934×10^{-8}	2.178×10^{-8}	2.865×10^{-9}	2.757×10^{-9}	2.079×10^{-8}	4.437×10^{-10}
25.	STDXD	1.432×10^{-7}	4.945×10^{-8}	9.429×10^{-9}	6.095×10^{-9}	–	1.300×10^{-9}
26.	SHDXE	1.150×10^{-7}	3.637×10^{-8}	4.603×10^{-9}	5.401×10^{-9}	4.200×10^{-8}	4.090×10^{-10}
27.	SCDTC	3.448×10^{-8}	1.434×10^{-7}	3.088×10^{-8}	4.428×10^{-9}	–	3.079×10^{-10}
30.	GHM4E	1.245×10^{-7}	6.042×10^{-8}	5.658×10^{-9}	3.212×10^{-9}	6.843×10^{-8}	2.179×10^{-10}
31	GHS4D	1.762×10^{-7}	6.970×10^{-8}	9.398×10^{-9}	7.986×10^{-9}	–	1.470×10^{-10}
32.	GHD4E	4.200×10^{-8}	2.192×10^{-8}	2.612×10^{-9}	2.005×10^{-9}	1.674×10^{-8}	5.099×10^{-11}
33.	GHD4D	7.676×10^{-8}	4.651×10^{-8}	6.852×10^{-9}	6.397×10^{-9}	–	9.440×10^{-11}
34.	GTM3D	8.520×10^{-8}	8.769×10^{-8}	5.989×10^{-9}	2.146×10^{-9}	–	2.011×10^{-10}
35.	GTM4D	1.372×10^{-7}	5.960×10^{-8}	4.002×10^{-9}	2.148×10^{-9}	–	1.580×10^{-10}
36.	GTD3D	1.322×10^{-7}	1.342×10^{-7}	3.638×10^{-8}	1.099×10^{-8}	–	1.134×10^{-10}
37	GTD4D	1.479×10^{-7}	7.888×10^{-8}	2.116×10^{-8}	1.100×10^{-8}	–	6.914×10^{-11}

Acknowledgements. We thank the Commission of the European Union (Environment and Climate Programme), the Electric Power Research Institute (EPRI) at Stanford, CA, USA, and the German Federal Ministry of Education, Science, Research, and Technology (BMBF) for financial support. We appreciate, in particular, the discussions and comments within the research cooperation of ESCOBA (European Study of Carbon in the Ocean, Biosphere and the Atmosphere) and of EPRI with the effort of building a community terrestrial biosphere model (CTBM). We acknowledge the cooperation with Dr Martin Heimann and Walter Sauf from the Max Planck Institute of Meteorology in Hamburg, and with Prof. Wolfgang Cramer and Dr Matthias Plöchl from the Potsdam Institute of Climate Research and their scientific and technical support. In addition, we thank Prof. Gerd Esser and 3 anonymous reviewers for their constructive criticism.

LITERATURE CITED

Apps MJ, Kurz WA, Luxmoore RJ, Nilsson LO, Sedjo RA, Schmidt R, Simpson LG, Vinson TS (1993) Boreal forests and tundra. Water Air Soil Pollut 70:39–53

Bray JR, Gorham E (1964) Litter production in forests of the world. Adv Ecol Res 101–157

Coupland RT (ed) (1979) Grassland ecosystems of the world: analysis of grasslands and their uses. Cambridge University Press, London

Esser G (1994) High Resolution Biosphere Model. Mitt Inst Pflökol Justus-Liebig-Univ Giessen

FAO/UNESCO (ed) (1974–1981) Soil map of the world I–IX, 1:5 000 000. UNESCO, Paris

Fung IY, Tucker CJ, Prentice KC (1987) Application of Advanced Very High Resolution Radiometer Vegetation Index to study atmosphere-biosphere exchange of CO_2. J Geophys Res 92(D3):2999–3015

Häger Ch, Würth G, Wagner U, Kohlmaier GH (1996) Responses in the growth of the northern forests to a CO_2 induced climatic change, as evaluated by the Frankfurt Biosphere Model (FBM). World Resour Rev 8(2):178–197

Haxeltine A, Prentice IC, Cresswell ID (in press) A coupled carbon and water flux model to predict vegetation structure. J Veg Sci

Heimann M, Keeling CD, Tucker CJ (1989) A three dimensional model of atmospheric CO_2 transport, based on observed winds: 3. Seasonal cycle and synoptic time scale variation. In: Peterson DH (ed) Aspects of climate variability in the Pacific and the Western Americas. Geophys Monogr 55:277–303

Holdridge LR (1947) Determination of world plant formations from simple climatic data. Science 105:367–368

Janecek A, Benderoth G, Lüdeke MKB, Kindermann J, Kohlmaier GH (1989) Model of the seasonal and perennial

carbon dynamics in deciduous-type forests controlled by climatic variables. Ecol Model 49:101-124

Jones HG (1992) Plants and microclimate—a quantitative approach to environmental plant physiology. Cambridge University Press, Cambridge

Kaduk J, Heimann M (1996) A prognostic phenology scheme for global models of the terrestrial biosphere. Clim Res 6: 1-19

Kindermann J, Lüdeke MKB, Badeck FW, Otto RD, Klaudius A, Häger Ch, Würth G, Lang T, Dönges S, Habermehl S, Kohlmaier GH (1993) Structure of a global carbon exchange model for the terrestrial biosphere: the Frankfurt Biosphere Model (FBM). Water Air Soil Pollut 70: 675-684

Kindermann J, Würth G, Kohlmaier GH, Badeck FW (1996) Interannual variation of carbon exchange fluxes in terrestrial ecosystems. Global Biogeochem Cycles 10:737-755

Kolchugina TP, Vinson TS (1993) Comparison of two methods to assess the carbon budget of forest biomes in the former Soviet Union. Water Air Soil Pollut 70:207-221

Köppen W (1936) Das geographische System der Klimate. In: Köppen W, Geiger R (eds) Handbuch der Klimatologie Vol 1, Part C. Gebr. Borntraeger, Berlin

Landsberg JJ (1986) Physiological ecology of forest production. (Applied botany and crop science series). Academic Press, London

Larcher W (1984) Ökologie der Pflanzen auf physiologischer Grundlage. Eugen Ulmer, Stuttgart

Lieth H (1975) Modelling the primary productivity of the world. In: Lieth H, Whittaker RH (eds) Primary productivity of the biosphere. Ecological studies 14. Springer-Verlag, New York, p 237-263

Lüdeke MKB, Badeck FW, Otto RD, Häger C, Dönges S, Kindermann J, Würth G, Lang T, Jäkel U, Klaudius A, Ramge P, Habermehl S, Kohlmaier GH (1994) The Frankfurt Biosphere Model: A global process-oriented model of seasonal and long-term CO_2 exchange between terrestrial ecosystems and the atmosphere. Part I. Model description and illustrative results for cold deciduous and boreal forests. Clim Res 4:143-166

Lüdeke MKB, Dönges S, Otto RD, Kindermann J, Badeck FW, Ramge P, Jäkel U, Kohlmaier GH (1995) Responses in NPP and carbon stores of the northern biomes to a CO_2-induced climatic change, as evaluated by the Frankfurt Biosphere Model (FBM). Tellus 47B:191-205

Lüdeke MKB, Ramge PH, Kohlmaier GH (1996) The use of Satellite-detected NDVI data for the validation of global vegetation phenology models and application to the Frankfurt Biosphere Model. Ecol Model 91:255-270

Lurin B, Cramer W, Moore B III, Rasool SI (1994) Global terrestrial net primary productivity. Global Change News (IGBP) 19:6-8

Matthews E (1983) Global vegetation and land use: new high-resolution data bases for climate studies. J Clim Appl Meteorol 22(3):474-487

Matthews E (1984) Global inventory of pre-agricultural and present biomass. Prog Biometeorol 3:237-246

Melillo JM, McGuire AD, Kicklighter DW (1993) Global climate change and terrestrial net primary production. Nature 363:234-240

Monsi M, Saeki T (1953) Über den Lichtfaktor in den Pflanzengesellschaften und seine Bedeutung für die Stoffproduktion. Jap J Bot 14:22-52

Nadler A (1994) Globales Mehrkompartimentmodell zur Kinetik der Streu- und Humuszersetzung im Hinblick auf die CO_2-Bilanz unter Berücksichtigung der Saisonalität von Temperatur, Niederschlag und Streufall. Diplomarbeit (Fachbereich Chemie), J. W. Goethe-Universität, Frankfurt am Main

Otto R (1996) Modellierung der terrestrischen Biosphäre im Hinblick auf den globalen Kohlenstoff- und Wasserkreislauf. Dissertation (Fachbereich Chemie), J.W. Goethe-Universität, Frankfurt am Main

Plochl M, Cramer W (1997) Coupling global models of vegetation structure and ecosystem processes—an example from arctic and boreal ecosystems. Tellus 47B:240-250

Potter CS, Randerson T, Field CB, Matson PA (1993) Terrestrial Ecosystem Production: A process model based on global satellite and surface data. Global Biogeochemical Cycles 7(4):811-841

Prentice IC, Cramer W, Harrison SP, Leemans R, Monserud RA, Solomon AM (1992) A global biome model based on plant physiology and dominance, soil properties and climate. J Biogeogr 19:117-134

Raich JW, Rastetter EB, Melillo JM (1991) Potential net primary productivity in South America: application of a global model. Ecol Appl 1(4):399-429

Reichle DE (ed) (1981) Dynamic properties of forest ecosystems. International Biological Programme, 23. Cambridge University Press, Cambridge

Rodin LE, Bazilevich NI (1968) World distribution of plant biomass. In: Eckardt FE (ed) Functioning of terrestrial ecosystems at the primary production level. UNESCO, Paris, p 45-52

Running SW, Hunt R Jr (1993) Generalization of a forest ecosystem process model for other biomes, biome-BGC, and an application for global-scale models. In: Ehleringer JR, Field CB (eds) Scaling physiological processes—leaf to globe. Academic Press, San Diego, p 141-157

Ryan MG (1991) Effects of climate on plant respiration. Ecol Appl 1(2):157-167

Saxton KE, Rawls WJ, Romberger JS, Papenndick RI (1986) Estimating generalized soil-water characteristics from texture. Soil Sci Soc Am J 50:1031-1036

Schmithüsen J (ed) (1976) Atlas zur Biogeographie. Meyers Großer Physischer Weltatlas, Vol 8. Bibliographisches Institut, Mannheim

Schnelle F (1985) 10jährige Mittel (Zeiträume 1963-1972 und 1973-1982) für 17 Phasen, die in 13 IPG beobachtet wurden. Arboreta Phaenologica 29:12-28

Shea DJ (1986) Climatological atlas: 1950-1979. Surface air temperature, precipitation, sea-level pressure, and sea-surface temperature (45°S-90°N). NCAR Tech Note 269+STR, NCAR, Boulder

Swift MJ, Healey IN, Hibberd JK (1976) The decomposition of branch-wood in the canopy and floor of a mixed deciduous woodland. Oecologia 26:139-149

Thornthwaite CW (1948) An approach toward a rational classification of climate. Geogr Rev 38:55-94

UNESCO (ed) (1973) International classification and mapping of vegetation. Ecology and conservation, Vol 6. UNESCO, Paris

Viereck LA, Dyrness CT, van Cleve K, Foote MJ (1983) Vegetation, soils, and forest productivity in selected forest types in interior Alaska. Can J For Res 13:703-720

Vörösmarty CJ, Moore B III, Grace AL, Gildea MP, Melillo JM, Peterson BJ, Rastetter EB, Steudler PA (1989) Continental scale models of water balance and fluvial transport: an application to South America. Global Biogeochem Cycles 3(3):241-265

Walter H, Breckle SW (1986) Spezielle Ökologie der Gemäßigten und Arktischen Zonen Euro-Nordasiens. Zonobiom VI-IX. Ökologie der Erde Vol 3. UTB für Wissenschaft, Große Reihe. Gustav Fischer, Stuttgart

Warnant P, Francois L, Strivay D, Gérard JC (1994) CARAIB: a global model of terrestrial biological productivity. Global Biogeochem Cycles 8(3):255–270

Webb RS, Rosenzweig CE, Levine ER (1993) Specifying land surface characteristics in general circulation models: soil moisture profile data set and derived water-holding capacities. Global Biogeochem Cycles 7(1):97–108

Wielgolaski FE, Bliss LC, Svoboda J, Doyle G (1981) Primary production of tundra. In: Bliss LC, Heal OW, Moore JJ (eds) Tundra ecosystems: a comparative analysis. IBP 25. Cambridge University Press, Cambrdige, p 187–225

Wisniewski J, Sampson RN (eds) (1993) Terrestrial biospheric carbon fluxes: quantification of sinks and sources of CO_2. Bad Harzburg, Germany, 1–5 March 1993. Reprinted from Water Air Soil Pollut 70(1–4). Kluwer Academic Publishers, Dordrecht

Zobler L (1986) A world soil file for global climate modelling. NASA Tech Ref 87802

Editor: G. Esser, Gießen, Germany

Manuscript first received: June 21, 1995
Revised version accepted: September 2, 1995